An Investigation of Active Microwave Remote Sensing of Summer Sea Ice in the Western Canadian Arctic

By

Kerri Warner

A Thesis submitted to the Faculty of Graduate Studies of

The University of Manitoba

in partial fulfillment of the requirements of the degree of

MASTER OF SCIENCE

Department of Environment and Geography

University of Manitoba

Winnipeg

ABSTRACT

Active microwave remote sensing is an important tool for classification of sea ice in polar regions. The aim of this research is to improve the understanding of microwave scattering that occurs during the advanced melt season, with a focus on multiyear ice (MYI). This was done using a combination of *in situ* C-Band scatterometer measurements, geophysical characteristics of ice, and Radarsat-2 data. Results indicate that it is difficult to differentiate between first year ice (FYI) and MYI during advanced melt but combinations of incidence angle and polarization exist that assist with this. It is known that the presence of liquid water governs microwave scattering, therefore further research investigating the variation of microwave backscattered signatures over a diurnal time period was conducted. These results indicate an inverse relationship between temperatures and microwave signatures. The overall results from this research show that summer MYI signatures are extremely variable and difficult to classify.

ACKNOWLEDGEMENTS

I would like to thank my supervisor, Dr. David Barber, and my graduate committee members Dr. Tim Papakyriakou and Mr. Kevin Sydor for their guidance throughout this research endeavor. Without your support this would not have been possible.

I would like to extend my thanks and appreciation to everyone involved with the various field seasons I had the opportunity to participate in, including the crew from the *CCGS Amundsen*. I would like to thank Jennifer Lukovich for her help. I would also like to especially thank Lauren Candlish and John Iacozza for their endless support, council and advice.

I would like to thank the ArcticNet program of the Network of Centre's of Excellence, the Canada Research Chairs (CRC) program, the Natural Sciences and Engineering Research Council (NSERC), and their Northern Science Training Program for their financial support.

To my friends and especially my family, Denise, George, Shannon and Eric. Thank you for being a constant source of encouragement and support.

TABLE OF CONTENTS

ABSTRACT ..... **ii**

ACKNOWLEDGEMENTS ..... **iii**

TABLE OF CONTENTS ..... **iv**

LIST OF TABLES ..... **vi**

LIST OF FIGURES ..... **vii**

CHAPTER ONE: INTRODUCTION **1**

1.1 Rationale and Context **1**

1.2 Objectives **2**

1.3 Outline **3**

Literature Cited 5

CHAPTER TWO: BACKGROUND **6**

2.1 Geophysical Properties of Sea Ice **6**

2.1.1 First Year Sea Ice 6

2.1.2 Multiyear Ice 12

2.1.3 Thermodynamic Properties of Sea Ice 16

2.2 Microwave Remote Sensing of Sea Ice **18**

2.2.1 Importance of Physical Properties of Sea Ice 20

2.2.2 Microwave Scattering in Sea Ice 20

2.2.3 Microwave Polarimetric Radar Measurements of Sea Ice 27

2.2.4 Radarsat Sensor 29

2.2.5 C-Band scatterometer 30

2.3 Chapter Conclusion **32**

Literature Cited 34

CHAPTER THREE: ON THE CLASSIFICATION OF MELT SEASON FIRST-YEAR AND MULTIYEAR SEA ICE IN THE BEAUFORT SEA USING RADARSAT-2 DATA **38**

Abstract 38
3.1 Introduction 39
3.2 Methods 42
3.2.1 *In situ* Observations 43
3.2.2 RadarSat-2 Observations 44
3.2.3 Data Products 47
3.3 Results and Discussion 48
3.4 Conclusions 58
Acknowledgements 61
Literature Cited 62
CHAPTER FOUR: DIURNAL MEASUREMENTS OF C-BAND BACKSCATTER FROM MULTIYEAR ICE IN LATE MELT SEASON 2011 67
Abstract 67
4.1 Introduction 68
4.2 Background 70
4.3 Study Area and Methods 72
4.4 Results and Discussion 77
4.4.1 Station S1 77
4.4.2 Station S2 83
4.4.3 Discussion 89
4.5 Conclusions 94
Acknowledgements 96
Literature Cited 97
CHAPTER FIVE: CONCLUSIONS AND RECOMMENDATIONS 101
5.1 Summary 101
5.2 Future Recommendations 104

LIST OF TABLES

Table 2.1: Parameters for the ProSensing C-Band scatterometer (from Isleifson, 2011)……. 32

Table 3.1: The date and time of acquisition, and pass direction for four Radarsat-2 images versus the date and times for the *in situ* sampling sites. First-year sites are denoted by #-F; multiyear sites by #-M…… 43

Table 4.1: Details (date, time, location) on the sampled stations……. 73

Table 4.2: Statistics (maximum, minimum and mean) for each sampling site S1 in each of the polarizations (HH, HV and VV) at the various incident angles…….. 81

Table 4.3: Statistics (maximum, minimum and mean) for each sampling site S2 in each of the polarizations (HH, HV and VV) at the various incident angles…….…….…. 89

Table 4.4: Mean backscattered Sigma naught (σ°) values obtained from Radarsat-2 data……..……..……. 92

LIST OF FIGURES

Figure 2.1: Salinity profiles of FYI (adapted from Maykut, 1985).……... 9

Figure 2.2: Schematic of FYI, including the frazil layer, the transition layer and the columnar layer (Cox and Weeks 1988)……... 11

Figure 2.3: Salinity profile of MYI in PSU, with the lowest salinity concentrations occurring at the surface layer, and gradually increasing with depth. (Adapted from Eicken et al., 1995).…….. 14

Figure 2.4: Straitgraphy of a MYI (Adapted from Eicken et al., 1995)……... 15

Figure 2.5: A summary of the experimental permittivity values for sea ice in the 4-5 GHz range. (Hallikainen and Winebrenner 1992)……..... 22

Figure 2.6: Illustration of "multiple scattering" (from Isleifson et al., 2009)……... 25

Figure 2.7: Backscatter interactions for multiyear ice, first year ice and open water. (Onstott, 1992)…….. 26

Figure 2.8: Summary of the seasonal evolution of radar backscatter ($\sigma°$) based on ERS and Radarsat-2 data for thick first year ice and multiyear ice in C-band (5.3 GHz). (Adapted from Barber 2005)…… 27

Figure 2.9: Synthetic Aperture Radar Imaging Concept……. 29

Figure 2.10: ProSensing Inc's Polarimetric C-Band scatterometer in position in the scatterometer shed on board the CCGS *Amundsen* (Isleifson)…… 31

Figure 3.1: Area map showing the *in situ* sampling stations and the ice conditions (obtained from CIS data from September 9, 2009)…….. 43

Figure 3.2: A Canadian Ice Service (CIS) ice chart (left) and RADARSAT-2 image (right) acquired on September 9, 2009 for an area west of Banks Island. The area outlined in brown in the ice chart represents multiyear ice and the area outlined in green represents thick first year ice. Based on visual inspection, the satellite imagery suggests that the same area is a mixture of FYI and MYI……... 46

Figure 3.3: Temperature profiles (A) and salinity profiles (B) for multiyear and first-year ice sites sampled during September 2009. First-year ice profiles are denoted by #-F, and multiyear ice profiles are denoted by #-M…… 50

Figure 3.4: Frequency distribution of sigma naught (σ°) from Radarsat-2 imagery acquired within a region of interest (ROI) for each ice type at different incidence angles. Sigma naught values for HH polarization are shown in the black bars; light bars represent the frequency distribution for HV polarization……. 51

Figure 3.5: Frequency distribution of sigma naught (σ°) from Radarsat-2 data acquired within a region of interest (ROI) showing the effects of HH polarization (a and b) and HV polarization (C and D) for each ice type at various incidence angles…… 53

Figure 3.6: Box plot displaying the effects of polarization for various ice types (FYI and MYI) and incidence angles (20°, 35° and 45°)…….…… 54

Figure 3.7: Box plot displaying the effects of incidence angles for various ice types (FYI and MYI) and polarizations (HH and HV)…….. 56

Figure 3.8: Box plot displaying the effects of ice type (FYI versus MYI) at 45° with HH polarizations (a) and HV polarizations (b)…… 57

Figure 4.1: Area map showing *in situ* physical sampling stations…… 74

Figure 4.2: Study footprint from the scatterometer's view for [2a] S1 (sampled PS-) on August 15 2011 and [2b] S2 (sampled PS-) on August 17, 2011…….…… 76

Figure 4.3: The diurnal cycling seen in various parameters at station S1 of (A) air temperature (on ice air temperature shown as points), (B) HH backscattering signatures, (C) HV backscattering signatures, and (D) VV backscattering signatures from sampling dates of 15 August to 16 August 2011…….……..…...… 79

Figure 4.4: Temperature profiles (A) and salinity profiles (B) for multiyear ice station S1 sampled during 15 August to 16 August 2011…….. 80

Figure 4.5: The diurnal cycling seen in various parameters at station S2 of (A) temperature, (B) HH backscattering signatures, (C) HV backscattering signatures, and (D) VV backscattering signatures from sampling dates of 17 August to 18 August 2011……... 84

Figure 4.6: Temperature profiles (A) and salinity profiles (B) for multiyear ice station S2 sampled from dates of 17 August to 18 August……..… 88

CHAPTER ONE: INTRODUCTION

This thesis presents new research in the use of microwave remote sensing for sea ice detection and segmentation. Examined in particular are the geophysical properties of ice during the summer melt season in addition to signatures obtained from an active microwave sensor. The primary goal of this study is to gain a better understanding of how the summer melt processes affect the geophysical properties of sea ice and in turn, examine their influence on active microwave signatures.

1.1 Rationale and Context

During the last decade the polar regions of our planet have received increased attention due to an accelerated decline in sea ice thickness (Rothrock et al., 1999), and extent (Kwok and Cunningham, 2010), in addition to the average age of sea ice (Maslanik et al., 2007). Of particular relevance is a transition from a predominantly multiyear ice (MYI) pack to a predominantly first year ice (FYI) pack (Kwok et al., 2009; Curry, Schramm, and Ebert, 1994). A loss in perennial ice in the polar regions during the summer months has resulted in an increase in the number of commercial and military ships that travel in the Arctic. With the increase in traffic there is a greater need for accurate detection, classification and segmentation of the ice types due to the hazards that exist for a ship travelling though sea ice, hydrocarbon exploration in Arctic coastal waters and indigenous use. As is described further below, the best method for sensing, categorizing and sectioning the types of ice is remotely sensed data.

Field campaigns conducted in the Arctic are hindered by adverse weather conditions, extended periods of darkness for over six months of the year, and the vastness

of the area. Research in the polar regions has however been facilitated by the use of satellites and other technologies. Microwave remote sensing is an effective method for studying sea ice as it can penetrate cloud cover, operate without solar illumination and can monitor some of the most remote areas in the world. This is significant as conditions in the Canadian Arctic are some of the harshest and most difficult to study. Space-borne radar systems have provided data on the state of the Arctic since the late 1970's, during which time significant changes in sea ice have been observed. While there has been a significant amount of research in the field of remote sensing of sea ice, there are comparatively few studies dedicated to the determination of ice type during the summer melt season. An accelerated decline in sea ice extent and related increase in traffic during summer however underlines the need for a greater understanding of sea ice conditions and type during the advanced summer melt period in the Arctic.

1.2 Objectives

The overall purpose of this study is to improve our understanding of the relationship between the geophysical state of sea ice and the active microwave signatures of late summer sea ice from the Radarsat-2 sensor and/or an *in situ* C-Band scatterometer. In order to achieve this goal, the following scientific objectives will be addressed through the study of sea ice conditions in the Beaufort Sea of the Canadian Arctic:

1. Investigate the geophysical properties of sea ice, specifically late summer melt season sea ice conditions;

2. Based on (1), quantify the microwave scattering differences between FYI and MYI in the late melt season and discuss potential solutions to increase their discrimination using new and emerging SAR technologies;

3. Expand on (2) by examining how small temperature changes affect the *in situ* multiyear sea ice microwave signatures in the summer season over a diurnal period to potentially improve discrimination of ice type.

1.3 Outline

This thesis is composed of five chapters. The first chapter introduces the rationale and outline for the thesis. The second chapter provides a literature review comprised of two parts. In part I, the geophysical properties of sea ice that are relevant to active microwave remote sensing are presented. This includes descriptions of the formation and melting processes that occur in FYI and MYI, and the thermo-physical properties of sea ice that have direct effects on the microwave signatures. In part II, a discussion on the history and use of active microwave remote sensing for sea ice detection is provided. This section also includes a description of the Radarsat-2 sensor and the C-Band scatterometer.

The third chapter consists of a manuscript written by Warner et al., (2012), entitled *On The Classification of Melt Season First-Year and Multiyear Sea Ice in the Beaufort Sea using Radarsat-2 data,* submitted to the **International Journal of Remote Sensing** in July 2012 and currently under review. This paper presents *in situ* physical measurements of sea ice and compares them with Radarsat-2 data. In this study we (1) determine whether the Canadian Ice Service (CIS) ice charts - using visual interpretation of SAR and related satellite products – adequately capture MYI in the late melt season; (2) compare *in situ* geophysical observations with sigma naught (σ°) values obtained from SAR data; and (3) examine whether different incident angles and polarizations can be used to improve the distinction of MYI and FYI in the late melt season.

Chapter four consists of a second paper written by Warner et al., (2012), entitled *Diurnal Measurements of C-band Backscatter From Multiyear Ice in Late Melt Season*

2011, which will be submitted to the **International Journal of Remote Sensing**. The paper is a comparison of two observational techniques. The first assesses data obtained from a C-Band scatterometer, placed at a site for a minimum of a 24-hour period in order to capture changes in the diurnal signatures of summer sea ice. This is then contrasted with the temperature data obtained from the meteorological tower as well as spot temperature measurements. The overall objective for this paper is to investigate how small diurnal temperature changes (typically less than 3°C) affect the *in situ* C-band microwave scattering from summer MYI. This will be addressed by (1) establishing how temperature-induced changes affect the geophysical properties of sea ice and how these affect the backscattering signatures obtained from a polarimetric C-Band scatterometer, (2) determining if there is a combination of optimal polarization and incidence angles for melt detection, and (3) investigating temporal variability in backscattered signatures from Radarsat-2 data to determine if there is an optimal time of day for floe discrimination.

In Chapter five conclusions are presented that summarize the findings of both manuscripts in this sandwich style thesis. Implications of this research for the scientific community and future directions necessary for the progression of knowledge of active microwave remote sensing during the important summer period in the Arctic are also discussed.

Literature Cited

Curry, J.; Schramm, J. and E. Ebert. 1994. Sea Ice-Albedo Climate Feedback Mechanism. Journal of Climate. Vol. 8. Pp. 240-247

Kwok, R. and G. F. Cunningham. 2010. Contribution of melt in the Beaufort Sea to the decline in Arctic multiyear sea ice coverage: 1993–2009. Geophysical Research Letters. Vol. 37. No. L20501. doi:10.1029/2010GL044678.

Kwok, R.; Cunningham, G. F.; Wensnahan, M.; Rigor, I.; Swally, H.J. and D. Yi. 2009. Thinning and volume loss of the Arctic Ocean Sea Ice Cover: 2003-2008. Journal of Geophysical Research. Vol. 114. No. C7. Pp. C07 005.

Maslanik, J.; Drobot, S.; Fowler, C.; Emery, W. and R. Barry. 2007. On the Arctic climate paradox and the continuing role of atmospheric circulation in affecting sea ice conditions. Geophysical Research Letters. Vol. 34. No. L03711. doi:10.1029/2006GL028269.

Rothrock, D. A.; Yu, Y. and G.A. Maykut. 1999. Thinning of the Arctic sea-ice cover. Geophysical Research Letters. Vol. 26. No. 23. Pp. 3469-3472.

CHAPTER TWO: BACKGROUND

2.1 Geophysical Properties of Sea Ice

The geophysical and thermodynamic properties of sea ice directly affect the wave propagation and scattering as well as the absorption and reflection of electromagnetic waves (Winebrenner et al., 1992; Barber, 2005; Walker et al., 2006). Sea ice is a heterogeneous mixture of ice, brine, solid salts and air bubbles (Ulaby et al., 1986), and these physical properties are highly variable both in space and time. There are constant changes in temperature, salinity and structure making sea ice a thermodynamically and dynamically active medium over a range of space and time scales. This is important when considering the objective of the thesis because these changes in the surface physical properties have effects on the wave propagation and interaction within the sea ice volume.

2.1.1 First Year Sea Ice

Providing a definition of first-year sea ice (FYI) is instrumental when considering the objective of the thesis. It is explained as ice with a thickness of 0.30 m to 2 m that forms during the freeze up season, beginning in late September and completely ablating during the following melt season (Kwok et al., 2009; Assur and Weeks, 1982).

Formation & Melt of FYI

The formation of FYI is highly dependent on the thermodynamic controls in the lower atmosphere and within the ice (Assur and Weeks, 1982). Sea ice begins to form when the surface temperature of the ocean falls to -1.86°C, otherwise known as the freezing temperature of seawater, which has a salinity of 34 PSU. An instability in the upper ocean layer leads to the transfer of heat from the lower layers to the ocean surface;

this is known as convective mixing. The surface layer of the ocean becomes super - cooled, allowing for the formation of frazil ice, resembling small needles and platelets. The ice begins to thicken as atmospheric temperatures continue to cool due to the heat exchange between the ocean and the atmosphere during this freeze-up period. As the season progresses, this frazil layer begins to freeze together forming a thin continuous layer of ice on the ocean surface, referred to as grease ice. Grease ice then accumulates and thickens over time until it begins to freeze into a solid ice cover.

Depending on atmospheric conditions, the surface characteristics of sea ice can vary. In calm conditions with no wind, the surface properties of FYI are quite uniform and level as the ice has not been exposed to the elements that would create surface deformation and resulting topography, such as wind and wave action. The grease ice thickens, forming a thin elastic crust layer, known as nilas ice. In rough ocean conditions, the frazil accumulates into rounded pans, called pancake ice. These pancakes collide with one another, causing an ice surface with raised ridges (Tucker et al., 1992). Regardless of the conditions, calm or rough, the pack ice eventually consolidates. This amalgamation of ice types is when congelation growth occurs, involving seawater freezing to the bottom ice from the upward conduction of heat (Weeks and Ackley, 1982).

Throughout the winter, the congelation process allows the newly formed ice to thicken and columnar ice to form at the bottom of the floe. The temperature gradient that exists during the growth period in all ice types is coldest at the air-ice surface interface and warmest at the ice-ocean interface (Thomas and Dieckmann, 2010). This is significant because it affects the surface properties of the ice and thus microwave signatures. As the ice continues to thicken throughout the cold season, the bulk salinity is

rejected downwards causing the surface to be fresher while the salinity concentration increases with depth, resulting in the classic 'C' shape of the salinity profile in young sea ice (Petrich and Eicken, 2010).

Beginning in late May/early June, warm temperatures cause the first-year ice to enter the melting stage. The melt causes the enlargement of brine and air pockets, which expand until they connect with one another forming vertical brine channels. As temperatures continue to warm, the snow on the surface of the ice melts; this melt water flushes salinity down through the newly formed brine channels, thereby reducing the salinity at the ice surface. Typically, first year ice does not survive the summer melt because of warmer atmospheric and oceanic temperatures.

Salinity of FYI

The salinity of young sea ice is determined by a complex mixture of pure ice, solid salts, air and brine (Anderson, 1958), resulting in seasonally-dependent salinity profiles for ice (figure 2.1, Maykut, 1985). The curves (A-D on figure 2.1) are typical for younger first year sea ice throughout its formation. During the freeze-up process liquid brine inclusions are trapped within the ice, making the salinity concentration much higher in younger ice (figure 2.1, A) forming a C-shaped profile. This is significant because salinity directly affects the dielectrics of the ice, which affects scattering signatures (section 2.2.2). The salinity of FYI is higher due to the fact that less drainage of the brine channels has occurred. As the ice thickens, brine rejection occurs both upwards and downwards, causing the salinity to decrease slightly (figure 2.1, B). As the ice continues to age and thicken, for example when it is approximately 1 m thick (figure 2.1, D), the salinity further decreases as the process of brine rejection persists as the ice grows. The

brine rejection that transpires creates a dense highly saline layer of liquid water directly below the newly formed ice and results in the formation of frost flowers on the ice surface (Carsey, 1992).

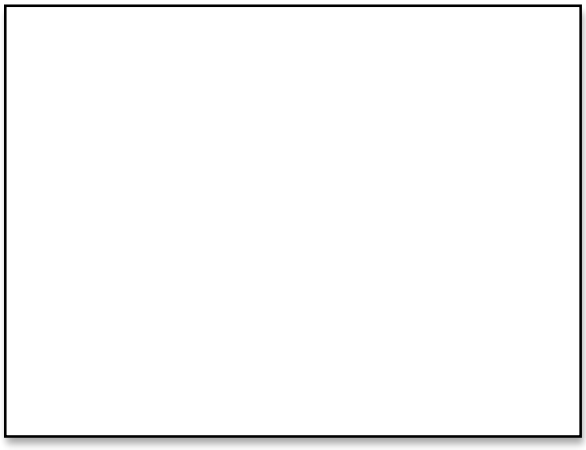

Figure 2.1: Salinity profiles of FYI (adapted from Maykut,1985). Labels refer to evolution in FYI formation and melt.

Refer to:

Maykut, G.A. 1985. The Ice Environment. Sea Ice Biota. Eds: R.A. Horner. Pp. 21-82. CRC Press. Boca Raton, FL.

Or

Tucker, W.; Perovich, D.; and A. Gow. 1992. Chapter 2: Physical Properties of Sea Ice Relevant to Remote Sensing from: Carsey, F. (Ed.). 1992. Microwave Remote Sensing of Sea Ice. Geophys. Monogr. Ser., vol. 68, P 13., AGU, Washington, D. C.

The presence of brine inclusions in sea ice microstructure is very important when analyzing the physical properties relevant to microwave scattering. Not only do the shape, size, content and number of inclusions affect the physical properties of the sea ice, but they also govern microwave properties and interactions of sea ice. The actual size and shape of the brine inclusions is highly dependent on the temperatures; in the freeze-up process, as the ice gets colder, the brine inclusions get smaller and reject the brine. This is important as these physical changes have direct effects on scattering signatures. Sea ice signatures with high salinity, such as FYI, have bright signatures and sea ice with low

salinity, such as MYI, have darker signatures during the cold season when everything is frozen.

Structure of FYI

First year sea ice can be identified by three distinct layers: frazil, transition and columnar layers. These layers have distinct physical characteristics due to differences in the growth processes for each, and can be easily determined when observing the microstructure of the ice (Tucker et al., 1992). These layers will be explained in depth below.

The surface layer of FYI consists of a frazil layer. Frazil ice has a fine-grained structure similar to needles (Cox and Weeks, 1988) with random orientations of the c-axes, brine and air inclusions (Cox and Weeks, 1988). The frazil layer thickness depends on the atmospheric conditions during which the ice was formed. In very windy areas frazil can accumulate up to a thickness of 1 m in pancake ice (rounded disks of slushy ice), whereas in calmer conditions this layer is typically quite thin, making up approximately 5% of the floe, with thicknesses ranging from 1- 10 cm in thickness at the surface (figure 2.2).

Directly below the frazil layer is the transition layer. Once the frazil layer has frozen together creating a porous and highly saline top layer, it limits the direction and freedom for continued growth of sea ice. This frazil layer insulates the warmer ocean from the cold atmosphere above. Seawater begins to freeze directly below this frazil layer, as a result of heat conduction upward through the surface layer of ice (Tucker et al., 1992). The transition layer is the result of the processes outlined above. Although it is

typically anywhere from 5 cm to 10 cm thick (figure 2.2), the transition layer can have lasting effects on sea ice or the environment. This transition layer is important during the freeze up process; the thickness of the transition layer paired with the thickness of the snow on the surface partially controls the movement of heat, thus affecting the rate of growth throughout the season.

The bottom layer of FYI consists of columnar ice, which is made up of a crystal structure that contains vertically elongated columns. The direction of growth is due to the direction of heat flow. During this growth period, heat escapes from below the sea ice at the ocean-ice interface, and rises towards the air-ice interface. Brine channels then separate these elongated columnar crystal features. This layer is typically the thickest out of the three main layers of first year sea ice (figure 2.2).

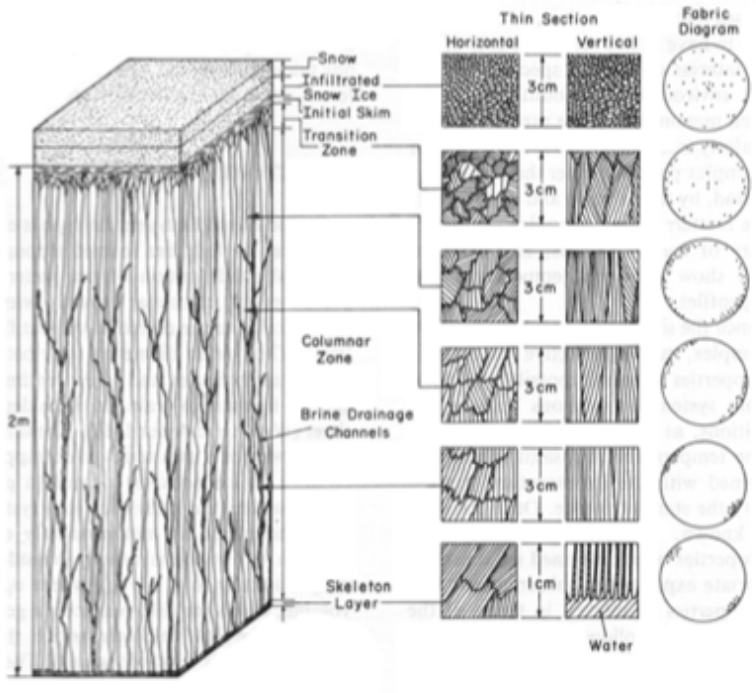

Figure 2.2: Schematic of FYI, including the frazil layer, the transition layer and the columnar layer (from Cox and Weeks, 1988)

2.1.2 Multiyear Ice

Multiyear ice is defined as ice that has survived at least one summer season (Petrich & Eicken, 2010). The average thickness for a multiyear floe can be anywhere from 3-5 meters, but in ideal conditions can reach a thickness of 12 m (Isleifson et al., 2009; Zwally and Gloersen, 2008; Weeks and Ackley, 1982). MYI has distinctive surface features known as hummocks and melt ponds (Untersteiner, 1968), which will be explained in detail below.

Formation & Melt of MYI

As with FYI, the formation of MYI is a result of the heat transfer from the ocean to the atmosphere and consists of columnar ice growing downward, thus further thickening the ice. The growth of MYI happens during the winter season in the Arctic, when temperatures are well below freezing.

The melt of MYI is very different than the melt that occurs in FYI. MYI is subjected to the warmer summer temperatures, causing significant changes in the physical and thermodynamic structure of the ice, especially at the surface layer. These melt processes affect the salinity, structure and surface properties of the multiyear sea ice, with implications for microwave scattering and signatures of sea ice.

Salinity of MYI

Major changes in the salinity of MYI typically occur during the melt season. As an ice floe ages and survives melt seasons, the bulk salinity concentration decreases over time. Tepid air temperatures warm the ice, allowing the brine pockets to expand and interconnect with one another, causing drainage of the brine down these vertical channels

in a process referred to as gravity drainage (Tucker et al., 1992). Melt water from the surface flushes through the pre-existing channels, which further enhances the desalinization of the ice through brine flushing. A noticeable decrease in salinity concentration occurs at the surface of multiyear ice within the top 50 cm (Tucker et al., 1992). MYI freeboard (wherein sea ice exists above the sea surface) has approximately 41 cm to 55 cm of height above FYI (Kwok et al., 2012) and this top portion of the floe is found to be very fresh; however, as the ice reaches the sea surface the salinity concentration increases with depth. A peak in the salinity typically occurs when the freeboard ends and the ice meets the sea surface (figure 2.3). The salinity profile shown in Figure 2.3 is typical of a MYI floe, where the salinity increases with depth to ~ 2 m (Eicken et al., 1995) due to the aforementioned freshening that occurs at the surface of MYI; brine is drained either by flushing or gravity drainage from the surface downwards. The freeboard that exists on MYI has a much lower salinity concentration than FYI. Differences in the surface properties of MYI and FYI allow for distinction between ice types during the winter season, since the microwave interaction occurs at the surface of the ice.

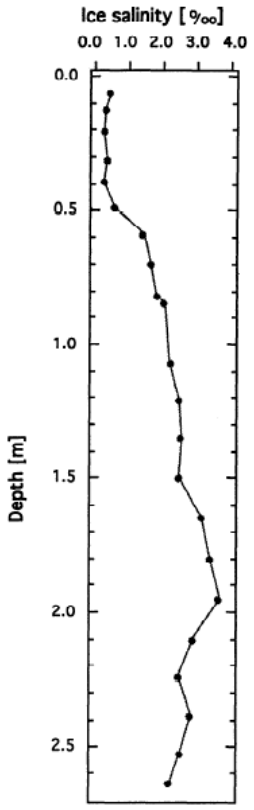

Figure 2.3: Salinity profile of MYI in PSU, with the lowest salinity concentrations occurring at the surface layer, and gradually increasing with depth (From Eicken et al., 1995.) Reproduced by permission of American Geophysical Union.

Structure of MYI

The crystal structure of multiyear ice is affected by the melt processes that occur during the summer melt season. In MYI, the main layers include a surface layer of deteriorated ice, a granular upper layer, a transition layer and a columnar layer (figure 2.4). The majority of the crystal retexturing occurs at the surface, in the deteriorated ice layer (Tucker et al., 1992). As a result, this layer is characterized by porous and brittle ice due to its exposure to the warmer temperatures during the summer. The changes that occur at the surface are crucial to the experiments in the thesis since this is where the signatures from the C-Band Radarsat-2 sensor and the C-Band scatterometer are obtained. (Microwave remote sensing will be discussed in section 2.2).

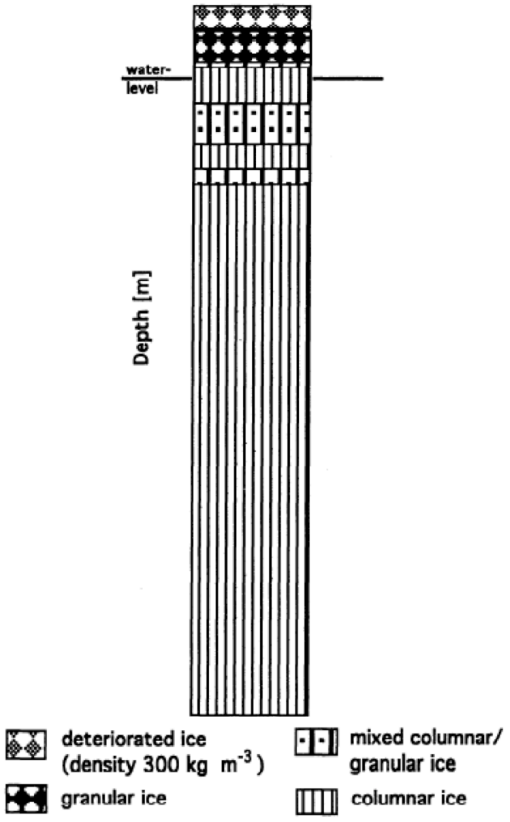

Figure 2.4: Stratigraphy of a MYI (From Eicken et al., 1995). Reproduced by permission of American Geophysical Union.

MYI has very different surface features than FYI structure, including the presence of rounded areas of high elevation resembling a weathered ridge known as hummocks. During the winter months, snow accumulates and forms drifts in the low-lying areas. As temperatures warm, these snow drifts melt causing a higher concentration of water, leading to the formation of fresh melt ponds appearing on the surface that are large enough to become wind-roughened. Due to differences in albedo of water and snow, more solar radiation is absorbed by the melt pond, causing it to increase in size, thus creating an even greater change of elevation between the hummocks and melt ponds (Maykut, 1985; Tucker et al., 1992). The depths of these melt ponds vary, but can be

anywhere from 50-100 cm. Occasionally they melt through a floe and can potentially fill with seawater (termed thaw holes), causing the salinity of the surrounding area to increase quite significantly (Tucker et al., 1992).

2.1.3 Thermodynamic Properties of Sea Ice

The thermodynamic processes that occur within sea ice refers to the amount of energy and how it moves throughout the sea ice volume and are governed by the energy balance across the ocean-sea ice-atmosphere (OSA) interface The coupled changes in thermodynamics and geophysics are referred to hereinafter as 'thermo-physical changes. There are 3 major parameters that are important in understanding the thermo-physical properties of sea ice: thermal conductivity, specific heat capacity and the latent heat of fusion. These three criteria control heat flow through the ice, which determines its growth. Since the thermo-physical state of the ice is inherently linked to electrical properties of the ice, it directly affects the signatures from radar.

The thermal properties of sea ice control the amount of heat that is able to move through the ice surface. The conductive heat flux, which occurs through the sea ice surface, F_c, is a product of the sea ice thermal conductivity λ_{si}, and the temperature gradient throughout the volume, dT/dz, (Petrich & Eicken, 2010):

$$F_c(z) = -\lambda_{si} (dT/dz)z$$

The thermal conductivity of sea ice is a function of temperature, the volume fraction of brine and the micro-structural arrangement (Petrich & Eicken, 2010) and is defined according to the relation (Untersteiner, 1961):

$$\lambda_i = \lambda_{pi} + \beta S/T$$

where λ_{pi} is the thermal conductivity for pure ice, $\beta = 0.13 \mathrm{Wm}^{-1}$, *S is* the salinity (ppt) and *T* is the temperature of the sea ice (°C). Differences in the thermal conductivity depend on the physical properties of sea ice. As an example, brine is about 25% of pure ice thermal conductivity (Makshtas, 1994). The presence of thermal conductivity within these brine cells causes a lag in the heating and cooling of the sea ice (Wadhams, 2002), meaning warm or high saline ice has a much lower thermal conductivity when compared to colder and lower saline ice.

Specific heat of sea ice is a function of temperature and salinity and refers to the amount of heat required to change state or change a specific amount of snow or sea ice by a certain temperature. It is highly dependant on the amount of water that is changing state as the temperature fluctuates and the specific heat capacity of each individual components including pure water, ice, brine and solid salts. The brine pocket sizes fluctuate according to temperature in order to maintain equilibrium within the system. The equations for this have been established (Schwerdtfeger, 1963 and Ono, 1967) and take into consideration the masses of pure ice and brine.

Latent heat is related to the energy from a thermodynamically-driven phase change within the sea ice; this is quite complex due to the coexistence of solid, liquid and vapor phases. It is defined as the heat released or absorbed during a phase change and is due to atmospheric temperatures fluctuations. This is important since as the seasons change, the physical properties at the surface of the ice change enough to cause differences in backscattering signatures.

The presence of snow can have significant effects on the growth and melt of the sea ice. Snow acts as a thermal blanket significantly slowing down the heat transfer

(Maykut and Untersteiner, 1971) during both growth and ablation seasons. During the early stages of formation, a thick snowfall can slow down the heat transfer between the ocean and the atmosphere, which in turn slows down the ice growth. During the melt season, the presence of a thick snow layer can slow the melt process by increasing the local surface albedo and thus reducing the amount of heat available from solar loading.

2.2 Microwave Remote Sensing of Sea Ice

As previously noted, sea ice responds to thermal forcing across the ocean-sea ice-atmosphere OSA interface which in turn affects its physical and electrical properties. It is this change to the thermo-physical state of the sea ice that renders synthetic aperture radar (SAR) and active microwave remote sensing such effective tools for classification and segmentation (distinction) of sea ice types. Furthermore, SAR and active microwave remote sensing can be used in the detection and classification not only of the geophysical state of the sea ice but also its thermodynamic state (Barber, 2005).

Remotely-sensed data began with the creation of NASA in 1958 (Masson, 1991). In the early stages of remote sensing, the majority of satellites operated in infrared or optical. The study of sea ice with optical sensors is however hindered by light source requirements, while adverse weather or thick cloud cover prevent the sensor from viewing the surface. Since polar winters in the Arctic are in complete darkness, optical sensors were not useful for nearly half the year. Thus, a technology that provided data in extreme climates, at high latitudes and through darkness was necessary.

As technology improved, microwave sensors were developed. There are numerous benefits to using microwaves, such as its ability to penetrate clouds, operate in

any solar illumination conditions, and monitor some of the most remote areas in the world. The original microwave sensors were mostly ground-based systems and located on aircrafts. Once the benefits of this technology were realized, the technology was brought up to space platforms and satellite sensors. The introduction of microwave remote sensing allowed researchers to study larger areas, and enabled the consistent collection of data and constant monitoring, yet with decreased spatial resolution.

Seasat, launched in 1978 (Massom, 1991), was the first satellite to use an active microwave remote sensor, which emits its own energy source; however, it failed after 108 days in orbit. Other microwave sensors have since been launched, providing an extensive data collection with coverage throughout the Arctic. Technological advancements and continuous upgrades have improved the quantity and quality of microwave data in the polar regions. Some of the parameters that can be estimated from the newer sensors include sea ice extent, type, concentration, motion and reflectance (Onstott, 1992). Since 1978 there have been numerous other satellite-based sensors launched including Radarsat-1 and Radarsat-2 , and there are plans for future satellites that will increase both the spatial and temporal coverage over the polar regions, such as the Radarsat Constellation. The Constellation mission will include a total of 3 satellites that will increase the availability and coverage of data in the Arctic. The Constellation mission will continue the Radarsat missions and is being designed so that it could potentially grow to a 6-satellite mission (discussed in 2.2.7). As technology continues to improve, a greater knowledge of sea ice conditions, such as extent, thickness, age or type, will be gained.

2.2.1 Importance of Physical Properties of Sea Ice

In order to understand how electromagnetic waves interact with sea ice, it is first crucial to understand how changes in the salinity, temperature, and structure affect microwave scattering signatures. The thermo-physical properties of sea ice directly affect the propagation of the radar waves in sea ice. These thermo-physical properties define the relative contributions of absorption, scattering and reflection of an electromagnetic wave throughout the sea ice volume. In turn, these thermo-physical properties control the dielectric constant (also known as complex permittivity) of the sea ice. The relative contribution of each component is a function of the dielectric constant of the sea ice at each progressive layer. Since sea ice is a heterogeneous mix of ice, air, brine and solid salts, the thermo-physical properties differ quite dramatically (both spatially and temporally) making it difficult to understand the relationship between thermo-physical properties and microwave signatures. Furthermore, as warming in the Arctic continues, MYI and FYI signatures will become increasingly difficult to differentiate.

2.2.2 Microwave Scattering in Sea Ice

In order to gain an understanding of scattering mechanisms, one must understand the dielectric properties of the volume. The dielectric properties refer to small displacements in the bound charges of the material when subjected to an electric field, leading to a general polarization of the medium. The dielectric constant defines the basic electrical property of a material and the amount of electromagnetic reflection, absorption and scattering that occurs within the medium. It is the dielectric constant of sea ice that

provides a basis for understanding of the thermodynamic and physical properties of the sea ice (Morey, Kovacs and Cox, 1984).

Dielectric properties are highly dependent on temperature, salinity, crystal structure and properties of the brine pockets, type of ice and the age of the ice (Sandven, Johannessen, and Kloster, 2006; Morey et al., 1984). As temperatures increase, the dielectric loss increases as precipitated salt goes back into solution, meaning the dielectric loss increases with salinity concentration. Multiyear ice has a lower dielectric loss compared to first year ice, which allows microwaves to penetrate deeper into the ice (Sandven, Johannessen, and Kloster, 2006), giving a volume backscattered signature (see section 2.2.4 for details on surface versus volume scattering). This volume-backscattered signature allows differentiation between MYI and FYI during the winter season.
The dielectric constant is expressed (by Debye) as:

$$\varepsilon = \varepsilon' + j\,\varepsilon''$$

where the real component ε' refers to the permittivity, which represents the ability of a medium to transmit incident energy, j represents $\sqrt{-1}$, and the imaginary component ε" represents the dielectric loss, which refers to the extinction of that energy (Langlois, A., 2006; Sandven, Johannessen, and Kloster, 2006; Hallikainen and Winebrenner, 1992). Differences in the physical characteristics between various ice types result in different dielectric properties.

Schwarz and Weeks (1977), Carsey et al., (1992), Onstott (1992) and Hallikainen and Winebrenner (1992) investigated the differences in the dielectrics between the various ice types. Figure 2.5 shows the dielectric values for FYI and MYI, at 4 GHz and 4.75 GHz respectively. Multiyear ice, which has a significantly lower salinity

concentration, has greater penetration depth and as a result has a lower dielectric constant. The dielectric loss of first year ice tends to decrease as the temperature increases; multiyear ice, however, has no clear trend. The general nature of the dielectric constant of both first-year and multiyear sea ice is discussed in greater detail elsewhere (Scharien et al., 2010; Vant, Ramseier, and Makios, 1978; Drinkwater and Crocker, 1988; Vant et al., 1974; Barber, Reddan and LeDrew, 1995; Schwarz and Weeks, 1977; Shokr, 1998) and is not duplicated here.

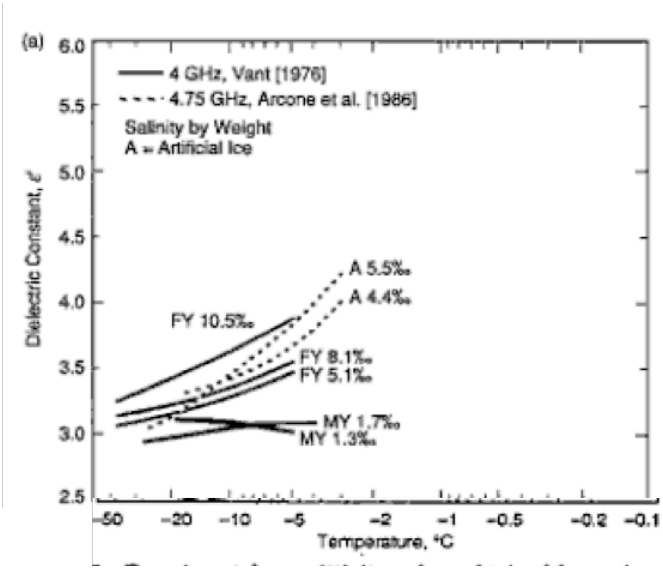

Figure 2.5: A summary of the experimental permittivity values for sea ice in the 4-5 GHz range. (Hallikainen and Winebrenner, 1992) Reproduced by permission of American Geophysical Union.

The scattering that occurs in sea ice is a complex process occurring at both the surface and within the ice volume. The thermo-physical state directly affects the physical characteristics of the sea ice, which in turn has an effect on the scattering of microwaves. There are differences in seasonal signatures due to the changing physical structure of cold frozen sea ice versus warm melting sea ice. The seasonal evolution of scattering that exists is highly dependent on the ice type and its thermo-physical state (Barber, 2005). To

simplify and describe the interaction process, researchers typically separate microwave scattering into surface and volume scattering. If the interface between two mediums has a high dielectric mismatch across this interface then surface scattering dominates (e.g. very salty first-year sea ice and the atmosphere). If the dielectric interface is fairly similar between two mediums then volume scattering dominates (scattering types defined in the following sections).

The interface dielectrics are defined by the Fresnel Reflection Coefficient, which is computed as a complex ratio of the dielectric properties of the two materials creating that interface. It is defined as (in this example air-snow or snow-ice) (Barber, 2005):

$$\Gamma_{HH} = \frac{\xi_2 \text{ x } \cos\theta - \xi_1 \text{ x } \cos\theta'}{\xi_2 \text{ x } \cos\theta + \xi_1 \text{ x } \cos\theta'}$$

Where ξ_1 and ξ_2 are the complex dielectric constants of the air and snow

$$\xi_1 = \frac{1}{\sqrt[2]{\varepsilon' + \varepsilon''}}, \text{ for material \#1 (air)}$$

$$\xi_2 = \frac{1}{\sqrt[2]{\varepsilon' + \varepsilon''}}, \text{ for material \#2 (snow)}$$

If the Fresnel Reflection Coefficient is large then surface scattering dominates and if it is small then volume scattering dominants. It is a measurement of the amount of radiation that is reflected at each interface between the adjacent mediums. The complexity occurs because of the differences of the dielectric properties between the various interfaces, which change as a function of both the spatial position in the sea ice (i.e. vertically and horizontally heterogeneous) and seasonally (i.e. the seasonal evolution and its control on

thermo-physical properties of the sea ice). Of particular interest in this study is the use of surface and volume scattering to differentiate between MYI and FYI, as described in the following sections.

Surface Scattering

Surface scattering occurs at the interface between the atmosphere and sea ice. If the surface of the ice is perfectly smooth, there is only incoherent backscatter. With a rougher surface the amount of scattering increases and becomes non-specular scattering. The dielectric constant of each medium and the difference between the various interfaces will strongly affect the scattering.

Surface scattering is much more common in newer ice due to the high salinity content of the surface that results in a dielectric mismatch and thus a high Fresnel Reflection Coefficient. As the brine rejected upwards freezes into frost flowers on the surface, the surface salinity increases. Due to a high number of brine and air inclusions, scattering primarily occurs at the surface. This phenomenon occurs in newly forming ice and has significant affects on the signatures due to high salinity.

Volume Scattering

In volume scattering the electromagnetic wave penetrates the medium and interacts inside the volume, which tends to be more common in older ice. The volume scattering is characterized by multiple scattering events occurring inside the medium. Similar to the surface scattering, the amount is governed by the dielectric properties of the volume of ice. A “mean wave” propagates through the background medium, which is termed the “coherent component” (Isleifson et al., 2009). As the wave travels through the medium, it interacts with the various scatterers such as the brine or air inclusions present

within the ice volume, creating an "incoherent component". The interaction of the wave with the various scatterers results in a re-radiation of energy (Isleifson et al., 2009). A multiple scattering scenario is a complex interaction in which the scattering is taking place with multiple inclusions within the medium (Figure 2.6). In figure 2.6a the wave is transmitted towards a half-space with many inclusions, each with different dielectric properties. Some of the energy from the electromagnetic wave is then reflected from the surface (figure 2.6b), while some of it penetrates into the lower half space with reduced intensity. The final panel (figure 2.6c) shows a wave that was scattered from the first inclusion and scattered from the surrounding inclusions.

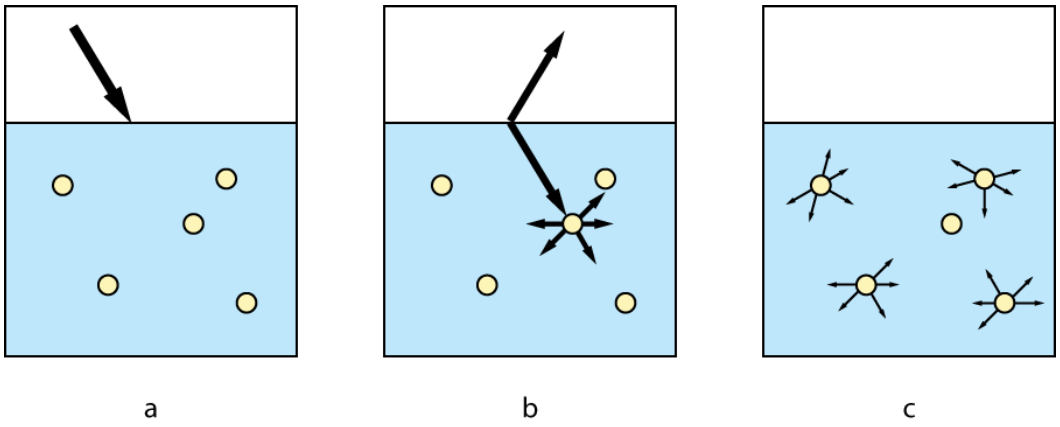

Figure 2.6: Illustration of "multiple scattering" (from Isleifson et al., 2009).

When determining what sort of scattering will occur, one must have an understanding of what type of scatterers are present in the medium, such as the presence of brine and air inclusions, their salinity concentrations and the temperature of the volume. The strength of the individual scatterers and the level of absorption within the medium determine the strength of the scattering. The strength of the scattering during the cold season allows for ice type identification.

Combined Scattering

Although separated for the point of discussion, surface and volume scattering often occur simultaneously. A typical backscattering signature from multiyear ice would be the result of surface-volume interactions taking place within the medium (figure 2.7), whereas typical backscattering signatures from first year ice are a result of surface scattering.

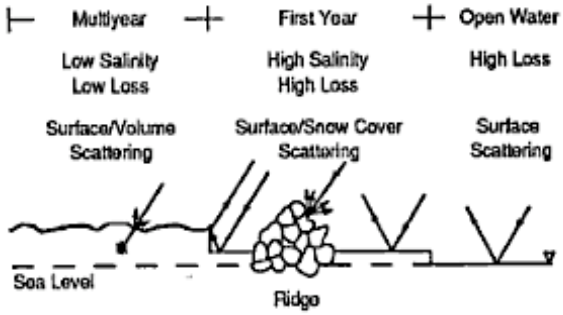

Figure 2.7: Backscatter interactions for multiyear ice, first year ice and open water. (Onstott, 1992)). Reproduced by permission of American Geophysical Union.

Since FYI has a high salinity concentration, it causes a large dielectric difference between the air and the surface, meaning the Fresnel Reflection Coefficient would be large, thus the dominant scattering process would occur from the surface. The scattering signatures for MYI are more complicated due to annual variations resulting from survival of MYI during summer. As MYI ages and thickens, the salinity concentration gradually decreases until the surface becomes near fresh. During the cold season, since the surface of the ice is near fresh, the Fresnel Reflection Coefficient would be smaller allowing the microwave to penetrate into the volume, allowing for volume scattering. During the warm season, melt processes causes a layer of water in liquid phase to appear on the surface of the ice. This layer causes MYI signatures to change to surface scattering as the water in liquid phase virtually masks the underlying ice.

2.2.3 Microwave Polarimetric Radar Measurements of Sea Ice

It is now understood that the thermo-physical state of the ice strongly affects the scattering; the microwave signature of the ice is affected by the dielectric constant, temperature, salinity and surface characteristics. The conditions in which the ice was formed, the season the measurements are being made, as well as the age of the ice affect the microwave properties and as a result the backscattered signatures.

It is important to differentiate ice types and open water in all seasons; however, during the summer season it is particularly important due to increased marine navigation. In calm open ocean conditions surface scattering dominates, and as the water roughness increases, it causes an increase in the backscatter of open water. New ice varieties, such as grease ice, dampen wave roughening of the ocean, which decreases scattering. Paradoxically the formation of young ice can increase scattering due to high salinity and a high Fresnel Reflection coefficient, but since the surface of the ice is smooth the scattering is dominant in the specular direction (away from the radar). Slightly thicker ice such as nilas ice, which is a thin sheet of smooth ice less than 10 centimeters, can have both a surface and volume scattering component. As the ice thickens and seasonal transitions occur, the signatures of the ice change. The seasonal evolution of backscatter for FYI and MYI has been defined for C-band SAR (Figure 2.8).

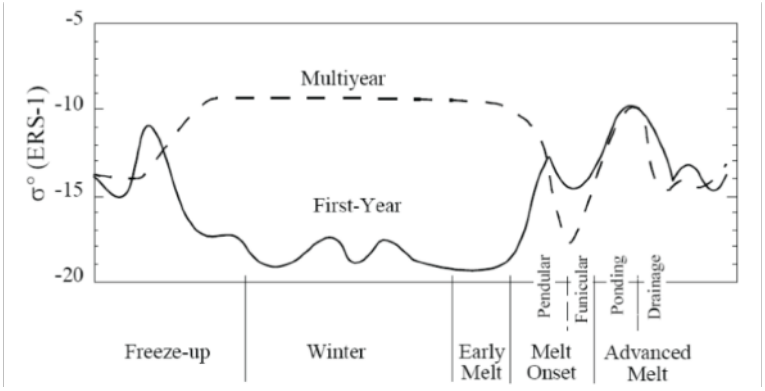

Figure 2.8: Summary of the seasonal evolution of radar backscatter (σ°) based on ERS and RADARSAT data for thick first year ice and multiyear ice in C-band (5.3 GHz). (Adapted from Barber, 2005). Reproduced with kind permission from Physics in Canada,

Monitoring the time series of SAR scattering allows scientists to gain a better understanding as to the unique temporal backscattering signatures and how they relate to the thermo-physical state of the sea ice as a function of season (Figure 2.8). In the winter season, there is a clear difference between the ice types, as FYI is dominated by surface scattering and MYI is dominated by volume scattering. However, as melt increases it becomes difficult to differentiate between the two ice types due to the presence of water in liquid phase and corresponding changes in the geophysical properties.

The use of radar measurements for monitoring sea ice conditions such as ice type, thickness and the thermo-physical state have proven to be extremely useful, but future work is necessary for continued refinement. The end goal of using this technology for studying sea ice, both in this thesis and elsewhere, is to obtain information on the physical parameters of the ice that affect the electromagnetic scattering mechanisms. Physical sampling of sea ice is necessary to understand its *in situ* characteristics for validation with remotely-sensed data (Skolnik, 1990). Frequency, polarization, incidence angles and specific aspects of the sea ice structure have an effect on the radar signatures (Onstott and Shuchman, 2004). There are certain signatures that are common to different ice types. For example, in the cold winter season MYI typically has more volume scattering, while FYI has more surface scattering. During the warm summer season or later in the melt process, FYI maintains surface scattering and MYI switches to surface scattering (as discussed in section 2.2.2)

Using polarimetric data has many advantages such as an improved ability to differentiate geophysical properties of the ice when compared to single polarization

(Drinkwater et al., 1992). In a basic monostatic radar system, the wave is emitted and received in the same polarization. For example, a wave transmitted vertically will be received vertically; this is referred to as a "VV return". This type of radar system provides co-polarized returns. Using a polarimetric radar system, the capability of data collection occurs in both vertical and horizontal (VV, HH, VH) returns is available, which is a large improvement over the single polarization systems.

2.2.4 Radarsat Sensor

The Radarsat sensor is a Synthetic Aperture Radar (SAR) system, with a single antenna mounted on a moving platform. Radarsat is an active sensor, meaning it emits microwave energy and measures the returned signal. A SAR sensor collects data using two parameters: range and azimuth. The range (cross track) is a measure of the 'line of sight' distance from the radar itself to the target and is determined by measuring the time from pulse transmission to the receiving of the returned echo from the target. The azimuth (along track) is perpendicular to the range. The combined range and azimuth provide a two-dimensional (2D) image of the surface properties of the medium (figure 2.9). An important part of Radarsat's physical structure is its large antenna, which transmits and receives the pulse as a sharp beam; the sharper the beam, the better the resolution.

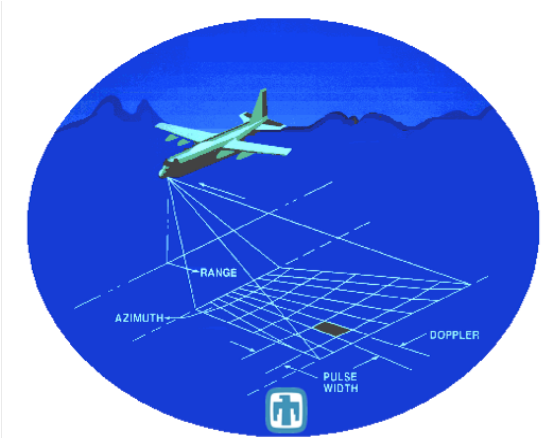

Figure 2.9: Synthetic Aperture Radar Imaging Concept (http://www.sandia.gov/radar/whatis.html)

Additionally, the brightness of the image is affected by the incidence angle, the surface roughness, moisture content, and dielectric constant. Data obtained during the advanced melt is ineffective in differentiating ice types and open water, as the layer of water in liquid phase that appears during the melt season blocks most wave penetration.

Radarsat-2 was launched in 2007 and is the most current application of scientific data collection used in the polar regions. It has a near polar orbit (798km) resulting in 14 orbits per day. The repeat cycle for an exact location is approximately twice a day at the poles. It has a frequency of 5.4 GHz (C-Band), allowing for good comparison with the C-Band scatterometer (section 2.2.5). The sensor is fully polarimetric using: HH, HV, VH, and VV, and has incidence angles varying from 10° to 60°. There are currently plans to launch a new series of sensors named the Radarsat Constellation, which will carry on the Radarsat mission.

2.2.5 C-Band scatterometer

The High Resolution Polarimetric C-Band scatterometer is an active radar system, developed by ProSensing Inc (figure 2.10). The unit operates in the C-Band frequency with a center frequency of 5.5 GHz and a bandwidth of 500 MHz (Table 2.1). It is dual polarized, allowing it to measure the fully polarimetric response of the ice and snow the VV, HH, HV and VH polarizations.

Figure 2.10: ProSensing Inc's Polarimetric C-Band scatterometer in position in the scatterometer shed on board the CCGS Amundsen (Isleifson).

The normalized radar cross section (NCRS) defined as σ°, is calculated from the data collected from the C-Band scatterometer, and is an average of the radar return over the sample area. The NCRS depends on the frequency, polarization, and angle of incidence, all of which are user-defined in the software. The NCRS also depends on the physical structure of the medium.

In this study, the C-band scatterometer was used during fieldwork in the Canadian Arctic and the data collected was interpreted and used in this thesis. The scatterometer was mounted on board the CCGS *Amundsen* during the 2009-2011 field seasons on the port side of the ship, at a height of approximately 8m with respect to the ice surface. This setup uses an automated positioner, which is controlled remotely from the dedicated laptop in the acquisition room on board the ship. At every ice station, the sea ice was scanned using the scatterometer. The elevation range was user defined from 20° to 60° in 5° increments, with the azimuthal measurements varying according to weather or ice conditions. The parameters defined in the software for the scans resulted in a keystone-

shaped scan. For data collected at the lowest incidence angle of 20°, 45°, and at the highest angle used for sampling, 60°, the corresponding fields of view are approximately 0.48m^2, 1.1 m^2, and 3.2 m^2, respectively.

Table 2.1: Parameters for the ProSensing C-Band scatterometer (from Isleifson, 2011)

Parameter	Value
Center Frequency	5.5 GHz
Bandwidth	500 MHz
Antenna Type	Parabolic Reflector
Antenna 3-dB Beamwidth	5.5°
Antenna Gain	28 dBi
Cross-polarization Isolation	>28 dB
Estimated Sensitivity	-40 dB
Transmit/Receive Polarizations	HH, VV, HV, VH

The C-Band scatterometer has many of the same parameters as Radarsat-2, such as the polarimetric capabilities, a similar frequency, and the defined variables (incidence angle). Both instruments operate in the same frequency making them an ideal comparison for imagery and microwave backscatter signatures. Both the C-Band scatterometer and the Radarsat-2 sensor were used throughout this thesis in order to investigate the use of C-Band microwave remote sensing for sea ice detection.

2.3 Chapter Conclusion

This chapter provides an overview of the physical properties of sea ice that are relevant to active microwave remote sensing. Differences in the geophysical properties, formation and melt, salinity, structure, and the thermo-dynamic properties of first-year and multiyear ice are presented, and their importance in distinguishing the microwave signatures obtained from each type with microwave sensors highlighted.

Sea ice is a thermodynamically and dynamically active medium and as a result there are constant changes in temperature, salinity and structure. The crucial differences between FYI and MYI that have major effects on microwave signatures are the differences in the salinity concentration, the presence of inclusions and the amount of water in liquid phase at the surface of the ice. Here it was shown based on previous studies that FYI is governed by surface scattering throughout the annual cycle, whereas MYI is governed by volume scattering during winter and surface scattering in late summer.

This chapter reviewed literature that investigated the relationships between the geophysical characteristics, the thermodynamic properties, the dielectrics and the microwave scattering properties of sea ice. In the next chapter, *in situ* physical measurements of FYI and MYI are analyzed, and a discussion as to whether it is possible to identify FYI and MYI during the melt season using Radarsat-2 data is provided.

Literature Cited

Anderson, D.L. 1958. A model for determining sea ice properties. Arctic Sea Ice. U.S. National Academy of Sciences – National Research Council. Pub. 598. Pp: 148-152.

Assur, A. 1958. Composition of sea ice and its tensile strength. Arctic Sea Ice. U.S. National Academy of Sciences-National Research Counsil, Pub. 598, 106-138.

Assur, A. 1960. Composition of sea ice and its tensile strength. U.S. Snow, Ice and Permafrost Research Establishment. Research Report-44.

Assur, A. and W.F. Weeks. 1982. Growth, Structure and Strength of Sea Ice. Cold Regions Research and Engineering Laboratory Monographs. Vol. 82. No. 1.

Barber, D.G. 2005. Microwave Remote Sensing, Sea ice and Arctic Climate. Physics in Canada. Vol. 61. Pp. 105-111.

Barber, D. G.; Reddan, S.P. and E. F. LeDrew. 1995. Statistical characterization of the geophysical and electrical properties of snow on landfast first-year sea ice. Journal of Geophysical Research. Vol. 100. No. C2. Pp. 2673–2686. doi:10.1029/94JC02200.

Carsey, F. (Ed.). 1992. Microwave Remote Sensing of Sea Ice. Geophys. Monogr. Ser. Vol. 68. 462 pp. American Geophysical Union. Washington, D. C.

Cox, G. F. N. and W. Weeks. 1988. Profile properties of under formed first-year sea Ice. CRREL Report CR 88-13. Hanover, N. H., Tech. Rep.

Drinkwater, M.R. and G.B. Crocker. 1988. Modeling changes in the dielectric and scattering properties of young snow covered sea ice at GHz frequencies. Journal of Glaciology. Vol. 34. No. 118. Pp. 274-282.

Drinkwater, M.R.; Kwok, R.; Rignot, E.; Israelsson, H.; Onstott, R. G. and D. P. Winebrenner. 1992. Chapter 24: Potential Applications of Polarimetry to the Classification of Sea Ice from: Carsey, F. (Ed.). 1992. Microwave Remote Sensing of Sea Ice. Geophys. Monogr. Ser., vol. 68, 462 pp., AGU, Washington, D. C.

Eicken, H.; Lensu, M.; Leppäranta, M.; Tucker III, W.B.; Gow, .A. J and O. Salmela 1995. Thickness, structure, and properties of level summer multiyear ice in the Eurasian sector of the Arctic Ocean. Journal of Geophysical Research. Vol. 100. No. C11. Pp. 22697-22710. doi:10.1029/95JC02188

Frankenstein, G. and R. Garner. 1967. Equations for determining the brine volume of sea ice from -0.5 ◦C to -22.9 ◦C. Journal of Glaciology. Vol. 6. No. 48. Pp. 943–944.

Hallikainen and Winebrenner, 1992. Chapter 3: The Physical Basis for Sea ice Remote Sensing from: Carsey, F. (Ed.). 1992. Microwave Remote Sensing of Sea Ice. Geophys. Monogr. Ser., vol. 68, 462 pp., AGU, Washington, D. C.

Isleifson. D. 2011. Simulation and Measurement Techniques for Microwave Remote Sensing of Sea Ice. Ph.D Dissertation. University of Manitoba.

Isleifson, D.; Langlois, A.; Barber, D.; Shafai, L. 2009. C-Band Scatterometer Measurements of Multiyear Sea Ice Before Fall Freeze-Up in the Canadian Arctic. IEEE Transactions on Geoscience and Remote Sensing. Vol. 47. No. 6. pp. 1651-1661.

Kwok, R.; Cunningham, G. F.; Wensnahan, M.; Rigor, I.; Swally, H.J.; Yi, D. 2009. Thinning ns volume loss of the Arctic Ocean Sea Ice Cover: 2003-2008. Journal of Geophysical Research. Vol. 114. No. C7. Pp. C07 005.

Langlois, A. 2006. Seasonal Linkages between Surface Energy balance, snow, geophysical properties and microwave remote sensing over first year sea ice: applications to snow water equivalent retrieval. Ph.D. Candidacy Exam. University of Manitoba.

Makshtas, A.P. 1994. Thermodynamics of Sea Ice in Physics of Ice-Covered Seas Vol 1, M. Lepparanta (Eds).

Maykut, G.A. 1985. The Ice Environment. Sea Ice Biota. Eds: R.A. Horner. Pp. 21-82. CRC Press. Boca Raton, FL.

Maykut, G. A. and N. Untersteiner. 1971. Some results from a time dependent, thermodynamic model of sea ice. J. Geophys. Res. Vol. 76. Pp. 1550–1575.

Maslanik, J. A.; Fowler, C.; Stroeve, J.; Drobot, S.; Zwally, J.; Yi, D. and W. Emery. 2007. A younger, thinner Arctic ice cover: Increased potential for rapid, extensive sea-ice loss. Geophysical Research. Letters. Vol. 34. No. L24501. doi:10.1029/2007GL032043.

Massom, R. 1991. Satellite remote sensing of polar regions. London: Belhaven Press. (book).

Morey, R.M.; Kovacs, A. and G.F.N. Cox. 1984. Electromagnetic properties of Sea Ice. Cold Regions Science and Technology. Vol. 9. Issue. 1. Pp. 53-75

Ono, N. 1967. Specific heat and heat of fusion of sea ice. In: Physics of Snow and Ice (H. Oura, ed.). Institute of Low Temperature Science, Hokkaido University, Sapporo, Japan. Vol. 1. No. 1. Pp. 599-610.

Onstott, R. G. 1992. Microwave Remote Sensing of Sea Ice: Chapter 5: SAR and Scatterometer Signatures of Sea Ice from: Carsey, F. (Ed.). 1992. Microwave Remote Sensing of Sea Ice. Geophys. Monogr. Ser., vol. 68, 462 pp., AGU, Washington,D. C.

Onstott, R. and R.A. Shuchman. 2004. SAR Measurement of Sea Ice from Chapter 3: Synthetic Aperture Radar Marine User's Manual.

Petrich, C. and H. Eicken. 2010. Sea Ice. 2nd Edition. Wiley-Blackwell. Chapter 2: Growth, Structure and Properties of Sea Ice.

Sandven, S., Johannessen, O. M. and Kloster, K. 2006. Sea Ice Monitoring by Remote Sensing. Manual of Remote Sensing: Remote Sensing of the Marine Environment. James F.R. Gower. 3rd Edition. Vol. 6. Bethedda: American Society for Photogrammetry and Remote Sensing. doi: 10.1002/9780470027318.a2320

Scharien, Randall K.; Geldsetzer, T.; Barber, D. G.; Yackel, J.J. and Langlois, A. 2010. Physical, dielectric, and C band microwave scattering properties of first-year sea ice during advanced melt. Journal of Geophysical Research. Vol 115. C12026. Doi: 10.1029/2010JC006257

Schwerdtfeger, P. 1963. The thermal properties of sea ice. Journal of Glaciology, Vol. 4. No. 36. Pp. 789-907

Schwarz, J. and W.F. Weeks. 1977. Engineering Properties of Sea ice. Journal of Glaciology. Vol. 19. No. 81. Pp. 499-531.

Shokr, M.E. 1998. Field observations and model calculations of dielectric properties of Arctic Sea ice in the microwave C-Band. Vol. 36. Issue 2. Pp. 463-478

Skolnik, M.I. 1990. Radar Handbook, 2nd edition. New York: McGraw-Hill.

Stroeve, J.; Holland, M. M.; Meier, W.; Scambos, T. and M. Serreze. 2007. Arctic sea ice decline: Faster than forecast, Geophysical Research Letters. Vol. 34. No. L09501. doi:10.1029/2007GL029703.

Stroeve, J.; Serreze, M.; Drobot, S.; Gearheard, S.; Holland, M.; Maslanik, J.; Meier, W. and T. Scambos. 2008. Arctic Sea Ice Extent Plummets in 2007. EOS, Transactions, AGU. Vol. 89. No. 2. Pp. 13-20

Thomas, D.N. and G.S, Dieckmann. 2010. Sea Ice: Second Edition. Wiley-Blackwell Publishing, Oxford, UK.

Tucker, W.; Perovich, D.; and A. Gow. 1992. Chapter 2: Physical Properties of Sea Ice Relevant to Remote Sensing from: Carsey, F. (Ed.). 1992. Microwave Remote Sensing of Sea Ice. Geophys. Monogr. Ser., vol. 68, 462 pp., AGU, Washington, D. C.

Ulaby, F.T.; Moore, R. K. and A. K. Fung. 1986. Microwave Remote Sensing: Active and Passive. Norwood, MA. Artech House Inc. Vol. 3.

Untersteiner, N. 1961. On the mass and heat budget of Arctic sea ice. Arch. Meteorol. Geophys. Bioklimatol. Ser. A. 12. Pp. 151– 182.

Untersteiner, N. 1968. Natural desalination and equilibrium salinity profile of perennial sea ice, Journal of Geophysical Research. Vol. 73. Pp. 1251-1257.

Vant, M.R.; Gray, R.B.; Ramseier, R.O. and V. Makios. 1974. Dielectric properties of fresh and sea ice at 10 GHz. Journal of Applied Physics. Vol. 45. No. 11. Pp. 4712-4717.

Vant, M.R.; Ramseier, R.O. and V. Makios. 1978. The complex dielectric constant of sea ice at frequencies in the range 0.1 to 40 GHz. Journal of Applied Physics. Vol. 49. No. 3. Pp. 1264-1280.

Wadhams, P. 2000. Ice in the Ocean. Taylor and Francis, NY, 368pp. (book)

Walker, N.P.; Partington, K. C.; Woert, V.; Street, M. L. and L. T. Towanda. 2006. Arctic sea ice type and concentration mapping using passive and active microwave sensors. IEEE Transactions on Geoscience and Remote Sensing. Vol. 44. No. 12. Pp. 3574–3584,

Weeks, W. and Ackley, S. 1982. The Growth, structure, and properties of Sea Ice. Cold Regions Research and Engineering Laboratory Monographs. Vol. 82 No. 1.

Winebrenner, D.P.; Bredow, J.; Fung, A. K.; Drinkwater, M. R.; Nghiem, S. V.; Gow, A. J.; Perovich, D. K.; Grenfell, T. C.; Han, H. C.; Kong, J. A.; Lee, J. K.; Mudaliar, S.; Onstott, R. G.; Tsang, L. and R. D. West. 1992. Microwave Remote Sensing of Sea Ice. Washington, DC. American Geophysical Union. Vol. 68.

Zwally, H. and Gloersen, P. 2008. Arctic Sea Ice Surviving The Summer Melt: Interannual Variability and Decreasing Trend. Journal of Glaciology. Vol. 54. No. 185. pp. 279-296.

CHAPTER THREE: ON THE CLASSIFICATION OF MELT SEASON FIRST-YEAR AND MULTIYEAR SEA ICE IN THE BEAUFORT SEA USING RADARSAT-2 DATA

This paper has been prepared and was submitted on July 17th, 2012 for peer review in the *International Journal of Remote Sensing*. This work represents a chapter in my thesis that was conceived, analyzed and reported by me as the senior author.

Warner, K., Iacozza, J., Scharien, R. K., and Barber, D.G. On the Classification of the Melt Season First-Year and Multiyear Sea Ice in the Beaufort Sea Using Radarsat-2 Data. International Journal of Remote Sensing. (in review). *Manuscript ID. TRES-PAP-2012-0529*

Abstract

Interpreting satellite microwave sea ice data during the melt season is difficult. Warm temperatures allow for a greater presence of water in liquid phase to be present at the surface and within the ice, causing the backscattering response for first-year ice (FYI) and multiyear ice (MYI) to be similar. Differentiating these ice types is important, especially during the summer season, due to the higher presence of seasonal marine traffic, ecosystem function and Inuit use of the marine icescape. In this paper, we investigate the similarities between geophysical, thermodynamic and dielectric characteristics of late season MYI and FYI, and discuss how this can lead to a false detection of MYI. The study uses Radarsat-2 data for ice detection in the summer season. This involved an analysis of co- versus cross-polarization (HH versus HV), various incident angles (20°, 35° and 45°), and ice types (FYI versus MYI). Statistical analyses of the measurements collected in 2009 identify the difficulty in differentiating ice types during this season. The results show the physical and electromagnetic properties of the ice surfaces are virtually identical with few differences in the scattering of microwave energy. We conclude with suggestions of how more effective differentiation of MYI and FYI types during summer may be accomplished.

3.1 Introduction

The marine cryosphere is a major part of the Arctic icescape that is currently facing dramatic changes. It is rapidly transitioning from a multiyear ice (MYI) dominated to a seasonal first-year ice (FYI) dominated system due to a faster and earlier melt (Kwok et al., 2009; Curry, Schramm, and Ebert 1994; Rothrock, Yu, and Maykut. 1999; Thomas and Dieckmann 2010). First-year ice is defined as seasonal or annual ice with a thickness of 0.30 m to 2 m that has formed during the freeze up season in late September (Kwok et al., 2009; Assur and Weeks 1982) and melts each summer. Multiyear ice has survived at least one summer season without completely melting, adding mass the following winter; average thickness varies from 3-5 meters, but can reach thicknesses of 12 m (Isleifson et al., 2009; Zwally and Gloersen 2008; Weeks and Ackley 1982). In late summer many different ice types can be present within a local area, such as surviving but decayed FYI, newly forming ice, MYI with hummocks and melt ponds present on the surface, and patches of open water. The replacement of MYI with younger sea ice is significant due to the changes in the fluxes of gases, mass and energy and the related impacts on the physical and biological components of the ocean-sea ice-atmosphere (OSA) interface and their interactions (Isleifson et al., 2009). The changes in the Arctic have implications on the overall global climate, the marine ecosystem and the ice management required for industry that operates in the Arctic marine system. Thus it is important that the types of sea ice and their concentrations be accurately differentiated and classified as to both geophysical and thermodynamic state (Barber 2005). The most practical way of doing this is space borne synthetic aperture radar (SAR).

The global climate is dependent on the conditions in the Arctic since changes in the sea ice have cascading effects to the global scale. The presence of a snow-covered sea ice creates a high albedo, the reflection of incoming solar radiation relative to what is absorbed, and is a major contributing factor to the Arctic climate and teleconnections to lower latitudes (Washington and Meehl 1986; Laine 2004; Rind et al., 1995; Curry, Schramm, and Ebert 1994; Covey, Taylor, and Dickinson 1991). The reflection of solar radiation modifies the movement of energy across the OSA interface. In recent years, there have been studies focusing on changes in ice regime from a predominant MYI to a FYI cover (Rothrock, Yu, and Maykut 1999; Hilmer and Lemke 2000). FYI is less likely to survive the summer melt causing an increased amount of open water and decreased albedo, which ultimately absorbs more incoming solar radiation, creating a positive ice-albedo feedback (Mysak and Venegas 1998; Rampal, Weiss, and Marsan 2009).

The presence and understanding of the two main ice types has a crucial influence on the industries (i.e. mining, oil exploration and fisheries) that are present in the Arctic and how they operate (Stewart et al., 2007; DeAbreu et al., 2003). Recent increased presence of industry is due to both decreasing sea ice hazards and global demand for resources. As the temperatures warm and the sea ice regime changes (Serrez, Holland, and Stroeve 2007; Johannessen, Shalina, and Miles 1999; Rigor and Wallce 2004; Comiso et al., 2008), the ocean becomes increasingly accessible and navigable, ultimately resulting in a higher presence and more traffic throughout the Arctic Ocean (Kerr 2002; Wilson et al., 2004). For navigation through the Arctic, a thick MYI floe would present very different threats than a FYI floe (Howell and Yackel 2004); thus

creating a need to accurately identify sea ice types during the summer, or exploration/development period.

Due to the high cost of conducting field campaigns in the Arctic, microwave remote sensing of sea ice is commonly used to study both the geophysical and thermodynamic state of sea ice (Barber, 2005). The behavior of microwaves interacting with ice types is related to the geophysical state (i.e., the partial fractions of brine ice and air) and the thermodynamic evolution of these variables seasonally. During the fall and winter period, surface scattering occurs within FYI as a result of the presence of high brine concentrations at the surface. Due to its lower salinity and fewer inclusions, MYI allows microwaves to penetrate into the sea ice leading to high volume scattering. During the cold season, the snow on both MYI and FYI surfaces is dry and cold without significant water in liquid phase. The differences in the scattering during the cold season allow the ice types to be distinguishable from one another in satellite data. As air temperatures increase, both sea ice types begin to go through the melt process. The snow on the surface of FYI melts, flushing the brine down through the opened channels. The surface of FYI in the late melt season has a greater presence of water, becoming near isothermal and saturated, affecting the scattering signatures (Barber 2005). Surface scattering remains the dominant mechanism in the melt season for both MYI and FYI. The key difference is that the MYI drains more effectively due to higher local topography. Little is known about the progression of the geophysical the electrical characteristics of the ice within the advanced melt season (Barber et al., 2009).

Although a considerable amount of research has focused on SAR remote sensing of sea ice, (Carsey 1992; Soh 1999; Drinkwater et al., 1991; Kwok, Rignot, and Holt

1992; Isleifson et al., 2009; Isleifson et al., 2010; Livingstone 1991; Nghiem and Bertoia 2001; Stofan 1995) most have examined the winter and fall seasons. Due to the considerable difficulty of working on late season ice, limited research has focused on this advanced melt summer season. Previous research has not examined the feasibility of using the various incidence angles combined with the polarization options available with Radarsat-2 products to improve separation of late season FY and MY signatures from SAR data.

Thus, the overall objective for this paper is to quantify the microwave scattering differences between FYI and MYI in the late melt season and to discuss potential solutions to increase their discrimination using new and emerging SAR technologies. This will be addressed by (1) determining if the Canadian Ice Service (CIS) ice charts (visual interpretation of SAR and related satellite products) capture MYI in the late melt season, (2) comparing in situ geophysical observations with sigma naught values (σ°) obtained from SAR data and (3) determining if different incident angles and polarizations can be used to improve the differentiation of MYI and FYI in the late melt season.

3.2 Methods

In order to address the objectives of this study, in situ measurements of late summer sea ice were made and compared with the CIS sea ice charts and satellite data. The Radarsat-2 SAR data were analyzed in conjunction with the in situ observations to determine if there are new approaches (e.g., polarization and incidence) which could be used to distinguish MYI from FYI in the late melt season.

3.2.1 *In situ* Observations

A total of four (two first-year and two multiyear) sea ice stations were sampled in situ in the Southern Beaufort Sea between September 1st and September 9th, 2009 (Figure 3.1) as part of an ArcticNet multidisciplinary study on board the icebreaker CCGS Amundsen. Sites were initially chosen using weekly ice charts provided by the Canadian Ice Service (CIS) and satellite data (Radarsat-2 data). Table 3.1 lists the dates, sample times, acquisition times and the location of the sites.

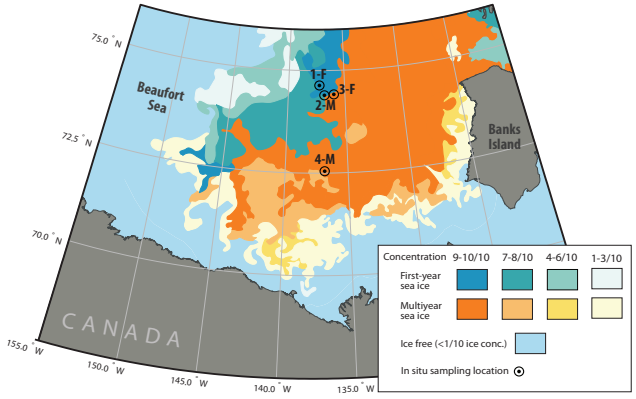

Figure 3.1: Area map showing the in situ sampling stations and the ice conditions (obtained from CIS data from September 9, 2009)

Table 3.1: The date and time of acquisition, and pass direction for four Radarsat-2 *images versus the date and times for the in situ sampling sites. First-year sites are denoted by #-F; multiyear sites by #-M*

***In Situ* Sampling**		**Location**			**Image Details**		
Station Name	Date	Latitude	Longitude	Sample Time (UTC)	Name	Acquisition time (UTC)	Pass
1-F	September 4, 2009	74.581	137.081	17:15	20090904_ 162456	16:24	Descending
2-M	September 5, 2009	74.403	136.433	16:00	20090905_ 155524	15:55	Descending
3-F	September 6, 2009	74.421	135.905	15:45	20090906_ 152531	15:25	Descending
4-M	September 9, 2009	72.513	136.738	16:50	20090909_ 153812	15:38	Descending

Upon arriving at a station, a visual estimation of ice type and ice thickness was done from the ship. After this visual observation, a minimum of two ice cores were extracted in situ, with depths varying from 70 to 175 cm, in order to collect physical samples to characterize the ice geophysics, thermodynamics and dielectrics. Cores were taken from the floe using a Kovacs Mark II coring system. Temperature profiles were measured from one core immediately after extraction by drilling a hole in the core at 10 cm intervals and placing a temperature probe into it, obtaining measurements that were accurate to within +/- .01°C. Salinity was measured from the second ice core. This core was cut into 10 cm sections, which were then placed into buckets and melted. Once melted, the salinity measurements were done using the conductivity and temperature readings obtained from a HACH SENSION5, a portable conductivity meter. The accuracy of the salinity measurements is +/- 0.01 practical salinity units (PSU).

The meteorological data were collected using the Automated Voluntary Observation Ship (AVOS) system onboard the CCGS Amundsen. This system measures temperatures (both air and sea), as well as other variables such as pressure, humidity, wind speed and direction and the GPS location. The only data used in this study was air temperature. The air temperature was collected every 10 minutes and then downloaded into a text file. The accuracy of the measurement is approximately ± 0.3°C.

3.2.2 RadarSat-2 Observations

Microwave scattering data from known ice types were obtained from the Radarsat-2 data (an example is seen in Figure 3.2). Radarsat is a C-Band active microwave sensor that has been used to examine sea ice characteristics over the last few decades (Radarsat 1 and 2). The sensor operates at 5.3 GHz within the microwave band

of the electromagnetic spectrum and has a wavelength of approximately 5 cm, allowing penetration depths from 0 (surface scattering) to about 30 cm (volume scattering and absorption) (Onstott and Shuchman 2004; Barber 2005). The swath width from ScanSAR Wide product (Radarsat-2) is 500 km across, with a spatial resolution of 50 m, with the option of obtaining data in single, dual or quad polarizations. For the purpose of this study, single co- (HH) and single cross- (HV) polarized ScanSAR wide data were acquired for each in situ sampling site (Table 3.1). Ice floes were chosen by physically sampling two first-year and two multiyear stations as well from aerial surveys using an electromagnetic induction (EMI) system (Prinsenberg, Peterson, and Holladay 1996). Following this, regions of interest (ROIs) were established within the satellite data that corresponded to the areas of known ice type. The ROIs included only one ice type, therefore the size of the ROIs varied between in situ sampling sites due to the differences in the size of the ice floe sampled. Sigma naught (σ°) statistics (mean, standard deviation, minimum and maximum) of the ROIs were extracted from the Radarsat-2 data. Sigma naught values are a conventional measure of the strength of radar signals reflected by the distributed scatterer, and are measured in decibels (dB). Due to the nature of the distribution of σ° values, a non-parametric Mann Whitney test was used to compare σ° distributions for ice types, different polarizations (HH and HV) and different incidence angles (20°, 35° and 45°). This statistical test does not make any assumptions about the underlying distribution of the data, and can be used with ranked or ordinal data.

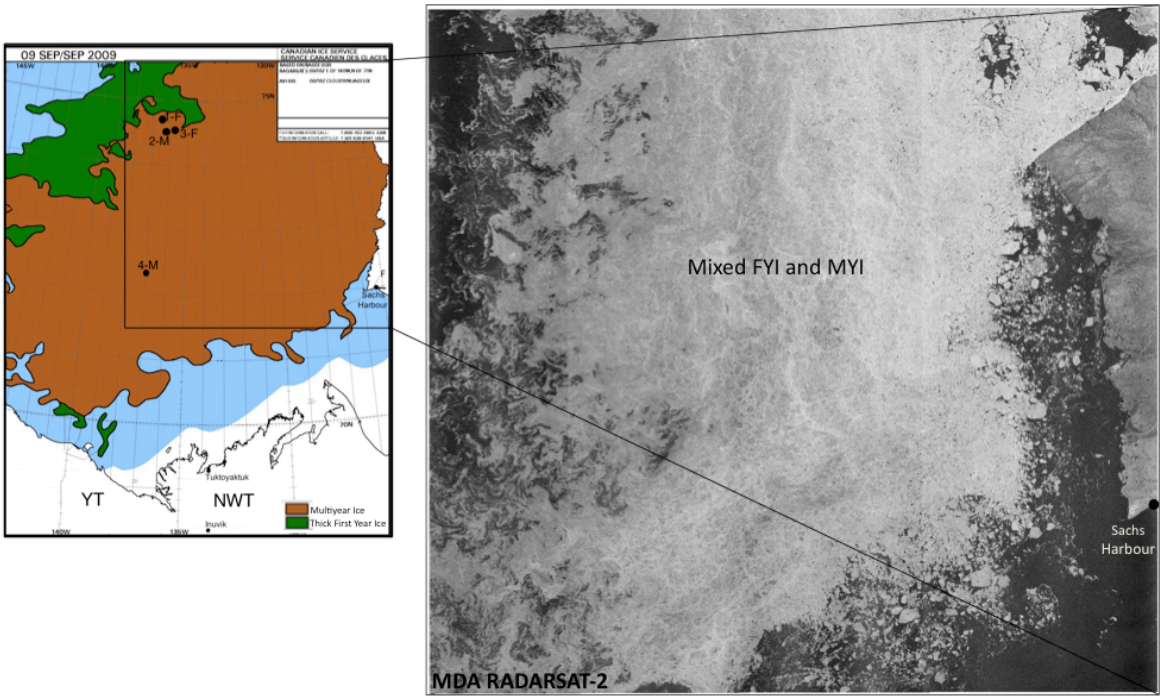

Figure 3.2: A Canadian Ice Service (CIS) ice chart (left) and RADARSAT-2 image (right) acquired on September 9, 2009 for an area west of Banks Island. The area outlined in brown in the ice chart represents multiyear ice and the area outlined in green represents thick first year ice. Based on visual inspection, the satellite imagery suggests that the same area is a mixture of FYI and MYI.

Aerial surveys of sea ice thickness and type were collected using a purpose built electromagnetic induction system (Prinsenberg, Peterson, and Holladay 1996) mounted on the Coast Guard's BO105 helicopter. These surveys were used to select additional areas of known MYI and FYI. In total, 20 sampling locations or ROIs were selected from the Radarsat-2 imagery (10 FYI and 10 MYI ROIs). The extraction of the Radarsat-2 sigma naught data from these ROI's resulted in the same statistics (mean, standard

deviation, minimum and maximum), and were then used for further analysis of the effects of polarization, incidence angles and ice types.

Co-polarized data (HH) is suitable for ice discrimination in the winter season (Onstott and Shuchman, 2004). This is when the surface temperatures of the ice are cold and the geophysical properties of each are unique, such as FYI having high, and MYI having low, surface salinities. Similarly, in the winter season, cross-polarized data (HV) is good for sea ice discrimination, and studies have shown that it can actually increase the range between MYI and FYI returns by 3 dB (Parashar 1974; Onstott, Moore, and Weeks 1979; Livingstone et al., 1983). This increase in range between the ice types for cross polarization data is a result of depolarization that occurs within the MYI volume, due to the presence of air bubbles. During the melt season, however, that discrimination can no longer be made due to major changes at the surface of the sea ice due to melt; the presence of melt water masks the volume scattering from MYI and causes the surface scattering to dominate.

3.2.3 Data Products

The Canadian Ice Service (CIS) publishes daily and weekly ice charts that are freely accessible on the CIS website (http://www.ec.gc.ca/glaces-ice/). These are based on an analysis and integration of many data sources, including shore, ship, aircraft-based visual observations and remote sensing devices in aircraft and satellites. Ice charts show a regional analysis of the ice conditions for a given area and date. These charts include estimations of ice type, stage of development, and form of ice, and are created by expert interpretation of these various data sources. The ice conditions are then plotted and described according to the International Standard Ice Code and the colour-coded format

using the World Meteorological Organization (WMO) Standard. The ice chart (Figure 3.2) nearest in date to the in situ sampling was chosen.

3.3 Results and Discussion

During the 2009 study, hourly air temperatures measured from the ship's meteorological tower were around 0°C, with a maximum of +1.2°C and a minimum of -5.6°C (mean = -1.4°C). Due to these conditions, the surface of ice was near the freeze-thaw point, resulting in higher concentrations of water in liquid phase at the surface of the ice during the day and refreezing at night. The ice was composed of a variety of FYI and MYI types interspersed with open water and new ice. Overall the ship-based observations from working in this icescape were significantly different than those presented in the CIS ice charts due to the difficulty in segmentation of MYI from FYI types. Details of this situation are presented elsewhere (Barber et al., 2009).

The first objective of this paper was to compare the CIS ice charts with the Radarsat-2 data products. Figure 3.2 shows the CIS ice chart for September 9th, 2009 (left) and a Radarsat-2 image from September 9th, 2009 (right) over the corresponding area. As shown in the ice chart the CIS forecasted the entire study area to be predominantly old ice or MYI, with a very little amount of FYI. The Radarsat-2 image clearly shows differentiation between land (Banks Island), open water and sea ice, however it classifies all of the ice as one type. The in situ observations confirmed that there was a mixture of rotten but surviving FYI and MYI. In this context rotten ice is defined following Barber et al. (2009), as remnant floes of multiyear and first-year each often covered by very young new-of-the-year growth sea ice. As seen in Table 3.1, a variety of ice types were physically sampled within the area that was predicted to be all

old ice. Multiyear ice was over-forecasted for this area in 2009 and this type of misclassification may have serious repercussions for shipping, oil and gas development of Inuit use of these regions. There needs to be further investigation into if MYI signatures can be differentiated from the FYI signatures and what are the geophysical and scattering characteristics that may allow for this separation?

The second objective of the paper was to compare the in situ physical observations with SAR data. The geophysical properties of the sea ice are important due to their effects on the microwave scattering. The ice temperature measurements were between -1°C and 0°C within the top 40 cm for both MYI and FYI (Figure 3.3a). The ice surface was warm, allowing for active brine drainage in both ice types (Golden et al., 1998). As temperatures increase above 0°C, the snow on the surface of the ice melted, freshening the surface as the water in liquid phase flushed the salinity downwards, through brine flushing and gravity drainage. The brine and air pockets began to expand with increasing temperatures until they meet up with one another, ultimately forming vertical brine channels. The salinity profiles for FYI are indicative of this process and result in late melt season sea ice with extremely low concentrations of salt at the surface increasing to a maximum of 3.8 PSU between 40 and 60 cm depth (Figure 3.3b). The salinity profiles of MYI are similar to the FYI, with salinity reaching a maximum of 3.4 PSU at 175 cm (Figure 3.3b). The low salinity seen at the surface suggests that both ice types can be considered near-fresh at the surface during the late summer. The surface properties of sea ice are extremely important when using microwave remote sensing to differentiate ice types. The low salinity and the presence of water in the liquid phase during the melt season causes changes in the scattering processes and signatures.

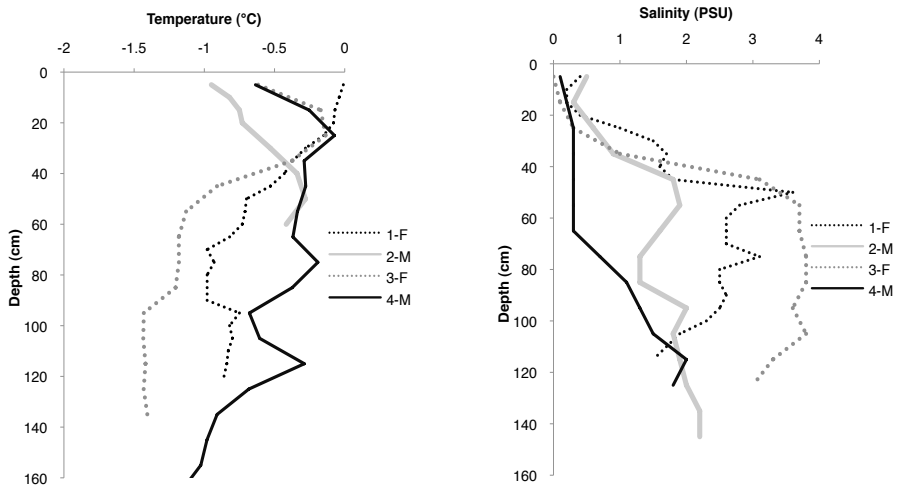

Figure 3.3: Temperature profiles (A) and salinity profiles (B) for multiyear and first-year ice sites sampled during September 2009. First-year ice profiles are denoted by #-F, and multiyear ice profiles are denoted by #-M.

To address the scattering at the sites with corresponding in situ measurements (Table 3.1), the analysis was restricted to only the four sample locations where we had on-ice measurements. In order to examine how microwaves interact with the ice surface, frequency distributions of σ° (dB) were obtained from four separate images at both co-polarization and cross-polarization (Figure 3.4). The various signatures obtained were separated according to incidence angle (20°, 35° and 45°) and ice type (FYI versus MYI). At the lower incidence angle (20°) there was no overlap between distributions in sigma naught values from the co-polarization and cross-polarization data (Figure 3.4a). The Mann Whitney statistical test confirms that the distributions of the two polarizations, HH versus HV at 20° are statistically different ($p<0.05$; Figure 3.4a). Similarly, the frequency distributions of co- and cross-polarizations at 35° and 45° incidence angles (Figure 3.4b, 3.4c and 3.4d respectively) are statistically different ($p<0.05$).

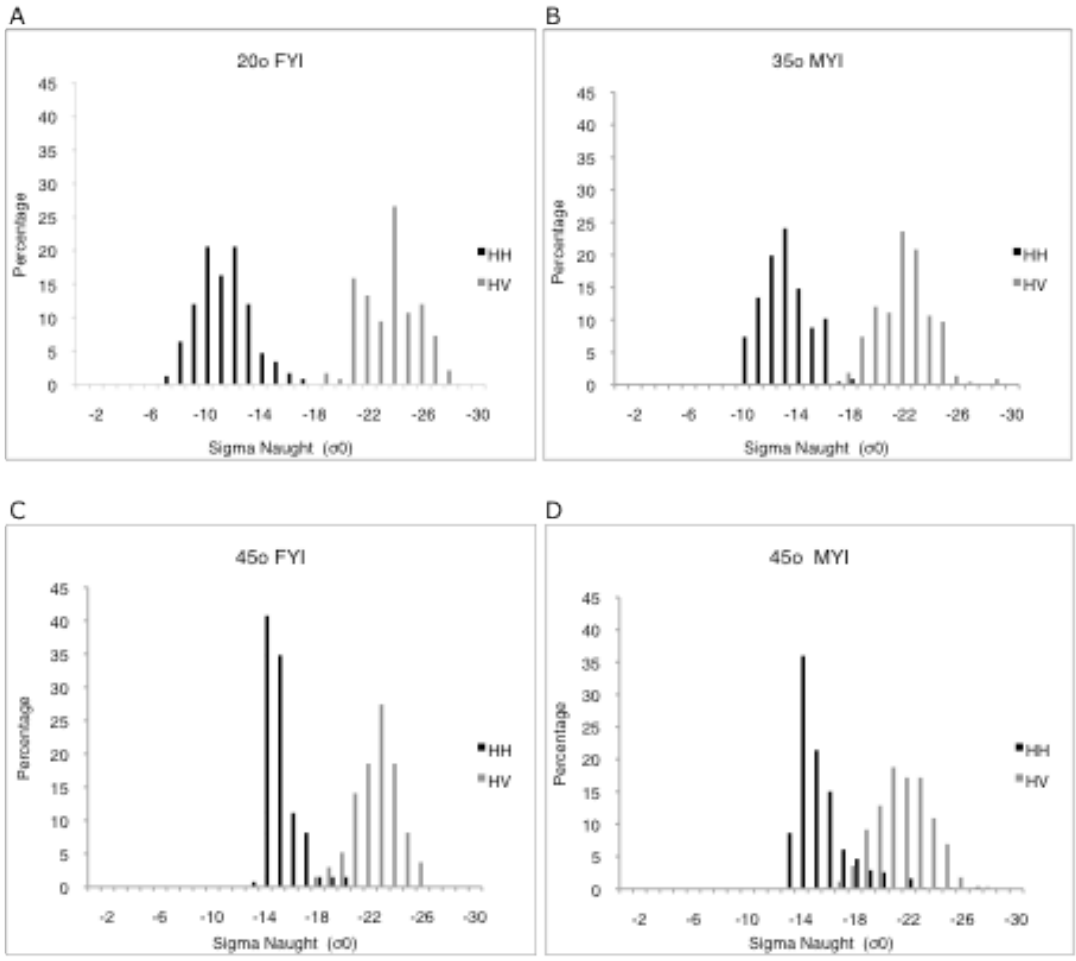

Figure 3.4: Frequency distribution of sigma naught (σ°) from Radarsat-2 imagery acquired within a region of interest (ROI) for each ice type at different incidence angles. Sigma naught values for HH polarization are shown in the black bars; light bars represent the frequency distribution for HV polarization.

The incidence angle defines the angular relationship between the radar beam and the ground and has a significant impact on σ°. Of note in Figures 3.4a and 3.4b are the similarities in backscatter magnitude at both polarizations between FYI and MYI, despite a 15° difference in incidence angle. Under the assumption that scattering from the MYI is not purely volume (some surface scattering occurs), the magnitude of backscatter would be expected to increase as the incidence angle steepens from 35° to 20°. This increase should occur at either polarization, resulting in a much greater backscatter magnitude for MYI than FYI, and class separability, at 20°.

Further analysis involved examining the impact of various incidence angles on the discrimination of ice types. When examining the differences between each individual polarization and ice type at the different incidence angles, it is clear that the relationship between incident angle and polarization is significant during the melt season. When comparing the incidence angles by ice types at a specific polarization, for example FYI at 20° and 45° incidence angles with HH polarization (Figure 3.5a), the analysis indicates that they are statistically different ($p<0.05$). The same results were obtained for the statistical analysis with FYI at 20° and 45° incidence angles with HV polarization (Figure 3.5c) ($p<0.05$). Similarly, when comparing MYI with HH polarization at 35° and 45° incidence angles (Figure 3.5b), and MYI with HV polarization at 35° and 45° incidence angles (Figure 3.5d), were proven to be statistically different ($p<0.05$). A comparison of all co-polarization frequency distributions (HH) (Figure 3.5a and 3.5b) at the various incidence angles was conducted and all were proven to be statistically different ($p<0.05$). Similar results are evident when examining cross-polarization (HV) data (Figure 3.5c and 3.5d). This analysis implies that the differences in incidence angles could be helpful in differentiating ice types during the melt season.

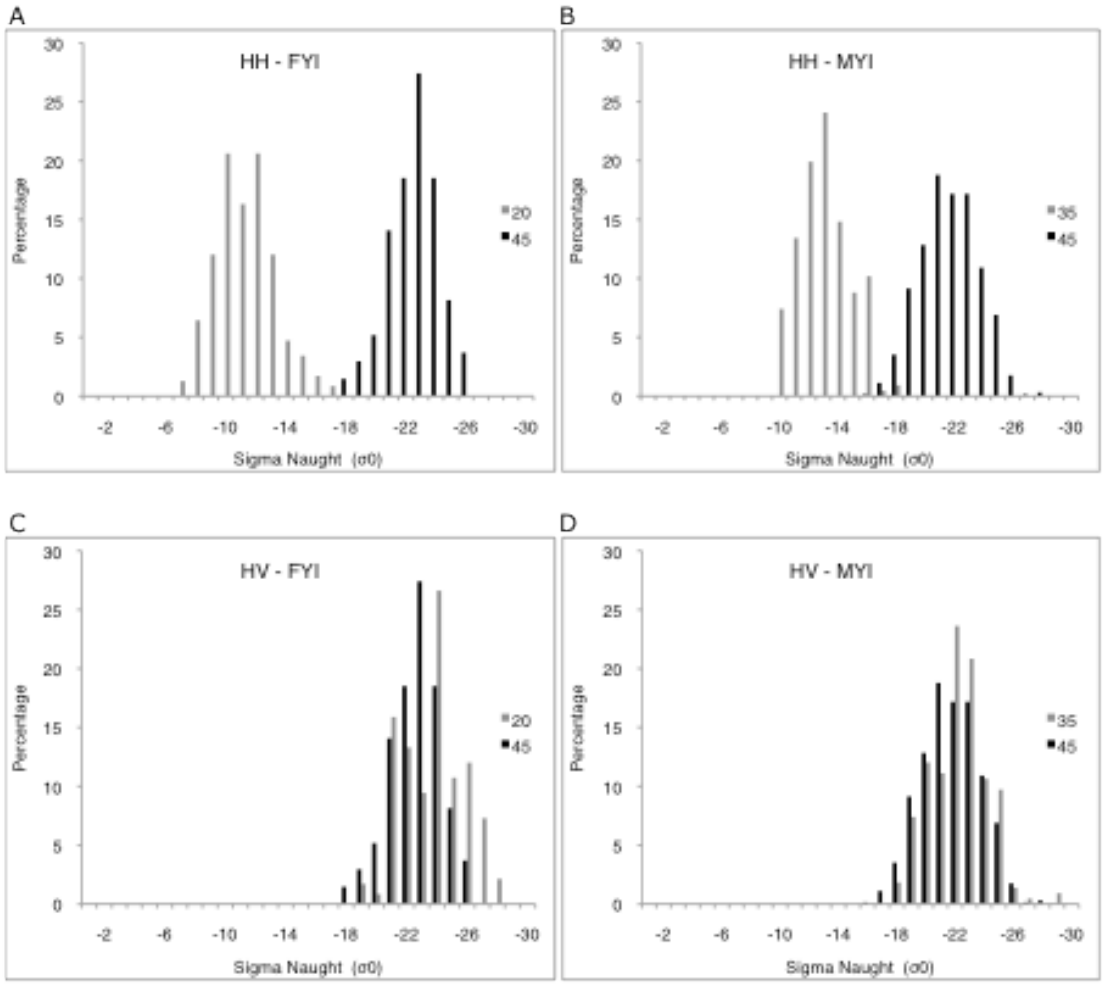

Figure 3.5: Frequency distribution of sigma naught (σ°) from Radarsat-2 data acquired within a region of interest (ROI) showing the effects of HH polarization (a and b) and HV polarization (C and D) for each ice type at various incidence angles.

The final objective for this paper was to determine if microwave scattering from SAR for different incident angles and polarizations could be used to segment MYI and FYI in the late melt season. The preceding analysis was limited to only four sample sites (two MYI and two FYI; Table 3.1). Here, we use the EM induction aerial survey data to locate unique FYI and MYI signatures in the Radarsat-2 data and extract ROI's at specific incidence angle, polarization and ice type.

Certain trends stand out when investigating the effects of polarization on SAR data (Figure 3.6). At the lower incidence angles, there is a large difference between co- and cross-polarizations (approximately 15 dB at 20°) (Figure 3.6a), however at the higher incidence angles, that difference decreases (8 dB at 45°) (Figure 3.6c and 3.6d). When comparing HH and HV polarizations for FYI at 20° (Figure 3.6a), they were proven to be statistically different from one another ($p<0.05$). Similar results were obtained from the analysis ($p<0.05$) when comparing HH with HV polarizations for MYI at 35°, FYI at 45°, and MYI at 45° (Figures 3.6b, 3.6c and 3.6d respectively); all were proven to be statistically different from one another. The results from the statistical analysis of the effects of polarization at the various incidence angles and ice types imply that it can aid in the classification of sea ice in the summer season.

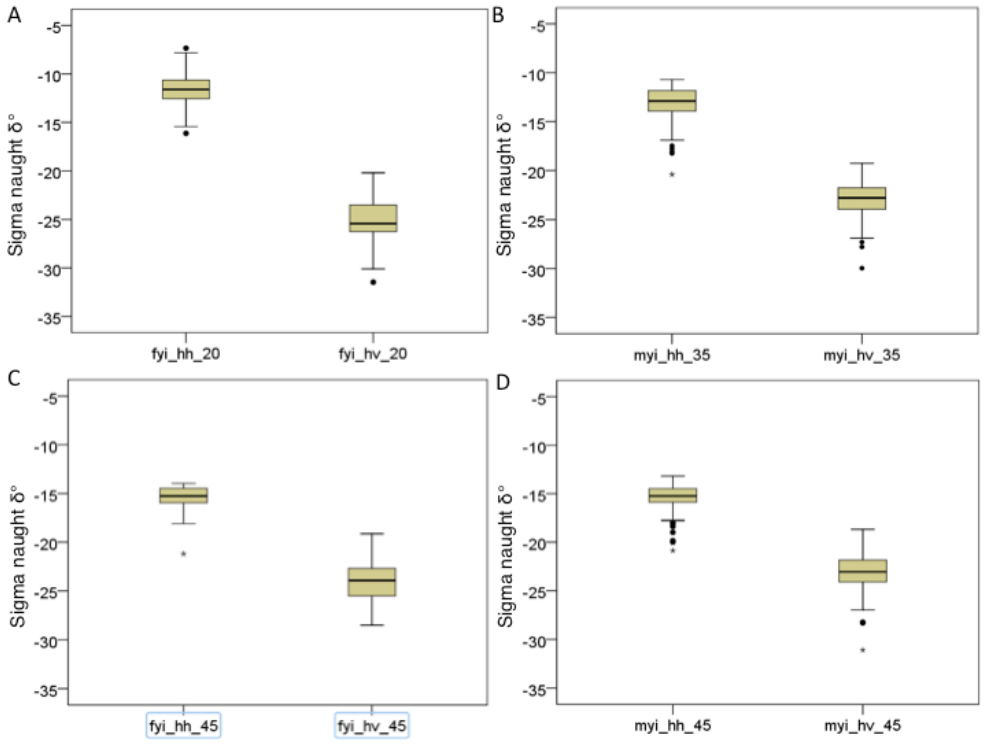

Figure 3.6: Box plot displaying the effects of polarization for various ice types (FYI and MYI) and incidence angles (20°, 35° and 45°).

The isolated effects of incidence angle in SAR data were also investigated (Figure 3.7). A statistical analysis of FYI signatures with an HH polarization, comparing 20° and 45° incidence angles (Figure 3.7a), was proven to be statistically different ($p<0.05$); similar results were seen with the same incidence angles with HV polarization (Figure 3.7b). When investigating the effect of incidence angle on MYI with an HH polarization, comparing 35° with 45°, the distributions were statistically distinguishable (Figure 3.7c). Examining the effects of MYI signatures with an HV polarization, comparing 35° with 45° (Figure 3.7d), the statistical analysis proved they were statistically indistinguishable ($p>0.05$). As the incidence angle increases with cross polarization (HV) imagery of MYI (Figure 3.7d), they remain statistically similar, meaning they could not be differentiated. This could be directly related to the similarities in the path length of the incident radar energy despite the different incidence angles. The results from the analysis of the effects of incidence angle at the various polarizations and ice types show that all were statistically different ($p<0.05$), except for the cross-polarization MYI signatures measured at the higher incidence angles (35° and 45°) (Figure 3.7d).

.

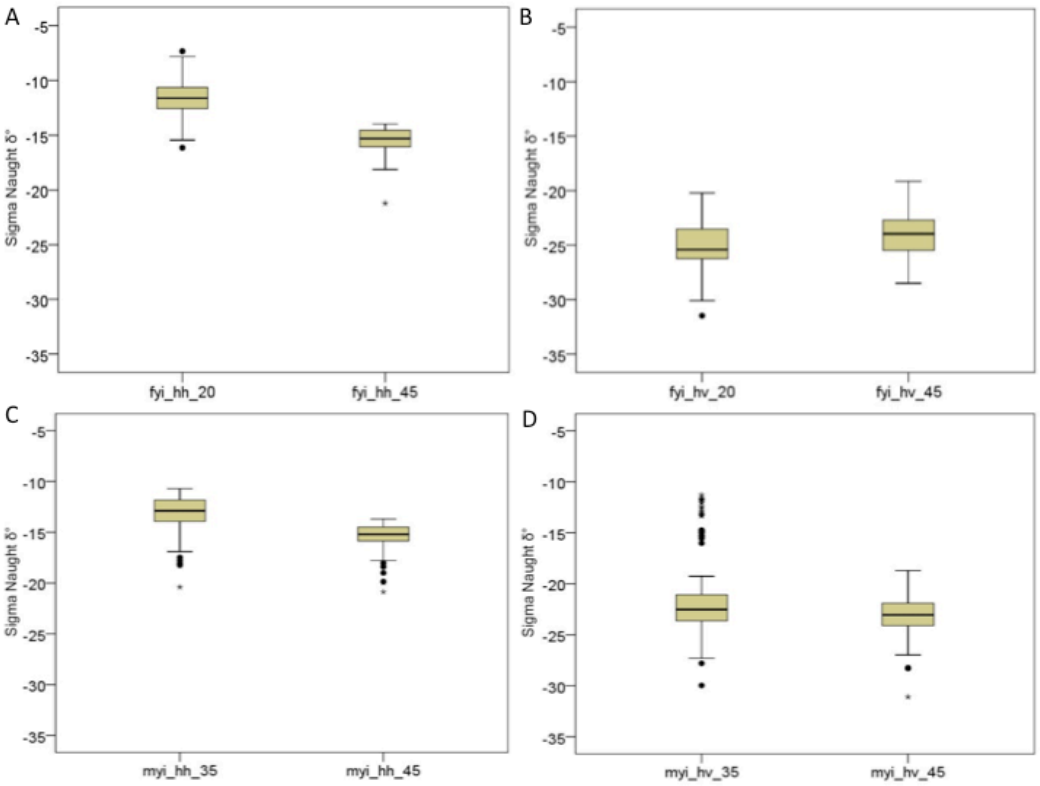

Figure 3.7: Box plot displaying the effects of incidence angles for various ice types (FYI and MYI) and polarizations (HH and HV)

A comparison of MYI versus FYI with a 45° incidence angle (Figure 3.8) was completed to determine the effect of polarization on classifying ice types in summer. Coincident FYI and MYI σ° data at the same incidence angle allowed for an investigation of different polarizations on discrimination of FY from MY ice types in summer. When comparing differences in ice types (Figures 3.8a and 3.8b), there is an overlap of the backscattered values, as seen in the σ° frequency distributions. The statistical analysis between co-polarized data (HH) shows that the σ° frequency distributions for FYI versus MYI are statistically the same ($p>0.05$). The same analysis of σ° frequency distributions for cross-polarized data (HV) shows that FYI and MYI are statistically distinguishable ($p<0.05$). When using co-polarized data (HH), Figure 3.8a shows that the different ice types at the same incidence angle and polarizations are statistically similar ($p>0.05$), suggesting this data cannot distinguish between MY and FY ice. However when using

cross-polarized data (HV), it was shown that the distributions were statistically different (figure 3.8b), suggesting that using cross-polarized data at a higher incidence angles can aid in the differentiation of MYI and FYI.

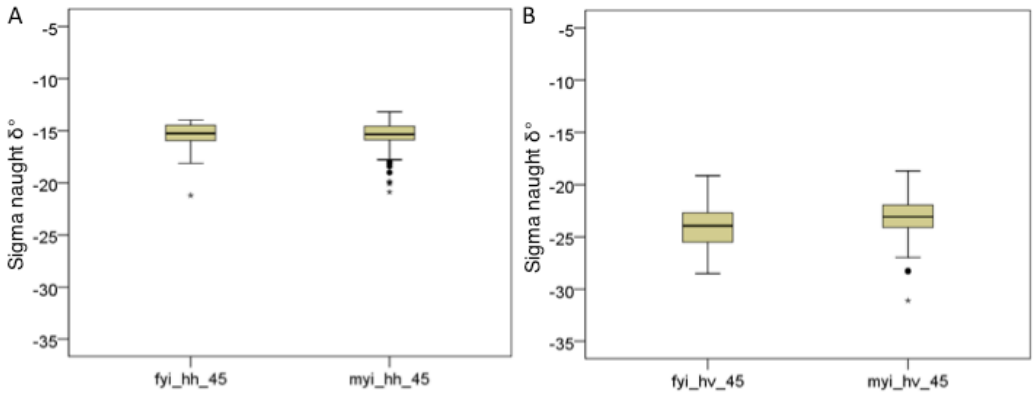

Figure 3.8: Box plot displaying the effects of ice type (FYI versus MYI) at 45° with HH polarizations (a) and HV polarizations (b)

During the summer season, the geophysical properties of MYI and FYI are very similar to one another, especially at the top 20 – 30 cm of the ice surface. Desalination from and replacement by air bubbles, combined with retexturing of the crystalline structure due to ablation and re-freezing, results in an uppermost FYI cover that is not entirely dissimilar to that of MYI (Eicken et al., 1994). The penetration of C-band energy into FYI and MYI differs considerably during the cold and dry season, when microwaves typically penetrate 20 – 30 cm into the freshened MYI and strongly backscatter from the volume, whereas penetration into saline FYI is minimal and backscatter is largely from the surface. During summer, the high concentration of water in liquid phase present in the uppermost layers of either ice type, combined with their similar physical properties, results in a convergence in penetration depths. For MYI, volume backscatter is masked

by the presence of liquid water, whereas for FYI backscatter is generally enhanced and there is a tendency for their backscatter signatures to overlap. Additional processes during late summer cause ambiguities in signatures. For FYI, it has been demonstrated that significant volume scattering can occur from the desalinated FYI when the volumetric wetness falls below 2%, and that enhanced surface scattering can occur from a surface layer of loosely decomposed ice grains, when these grains are disaggregated from the melting ice cover and wetted by liquid melt water exceeding ~ 1% wetness (Scharien et al., 2010). In a microwave scattering context, differences between ice types is thus more attributable to differences in the large scale features of each type and the role of these features on modifying the local incidence angle of the radar beam. At a larger scale, MYI is distinguishable by the effect of its hummocky terrain and the presence of deformation features, with features acting to steepen the local incidence angle and enhance backscatter. Conversely, FYI is distinguishable by its relatively smooth texture, the absence of hummocks and deformation features, and the greater occurrence of melt ponds (Eicken et al., 2004). All of these factors will either limit or enhance the discrimination of ice types during summer, thus requiring empirical examination as presented here.

3.4 Conclusions

The objectives of this paper included quantifying the microwave scattering differences between FYI and MYI in the late melt season and to establish possible solutions to increase their discrimination using SAR data. This was discussed by (1) determining if the Canadian Ice Service (CIS) ice charts and Radarsat-2 data (visual interpretation of SAR and related satellite products) correctly separated FY and MY in

the late melt season, (2) comparing in situ geophysical observations with sigma naught values (σ°) obtained from SAR data and (3) establishing if microwave scattering from SAR for different incident angles and polarizations can be used to differentiate MYI and FYI in the late melt season.

The results showed that it is difficult to differentiate between ice types using Radarsat-2 data during the late summer season due to the changing physical properties of the ice. This study involved the analysis of ScanSAR satellite data from Radarsat-2; the backscattering signatures (σ°) were obtained and used to determine if there were differences between the signatures of ice types (FYI versus MYI), as well as the differences seen from various incidence angles (20°, 35° and 45°) and polarizations (HH versus HV).

Comparing the σ° frequency distributions from the different polarizations (HH versus HV) for the same ROI suggested that the distributions were all statistically different ($p<0.05$), at all incident angles (Figure 3.4 and Figure 3.6). This confirmed that polarization partially governs wavelength behavior and as a result, the interaction with the surface. The statistical analysis of the differences in polarization implies that they may aid in the differentiation of the different sea ice types during the melt season.

The analysis of the incidence angles (20°, 35° and 45°) compared with polarizations confirmed that the σ° frequency distributions were statistically different from one another (Figure 3.5). The near range incidence angles (20°) would be more helpful in attempting to differentiate ice types when compared to the far range incidence angles (45°). The statistical analysis implies that incidence angle would have an effect on sea ice differentiation during the summer season. A second analysis of the effects of

incidence angle (Figure 3.7) determined that again, incidence angle (Figure 3.7a, 3.7b, 3.7c) was statistically different except when analyzing data in a higher incidence angles (35° and 45°) using cross polarized data (HV) (Figure 3.7d), they were statistically the same ($p>0.05$).

A comparison of the ice types (FYI versus MYI) was conducted (Figure 3.8), and the co-polarized data (HH) (Figure 3.8a) was proven to be statistically indistinguishable ($p>0.05$), meaning at 45°, these data were not able to differentiate between FYI and MYI. However, the cross-polarized data (HV) (Figure 3.8b) was proven to be statistically distinguishable ($p<0.05$), implying ice type also has a significant affect on the $\sigma°$ signatures obtained from the Radarsat-2 data. Due to the complexity of this data during the melt season, C-Band data has significant difficult in definitely separating the ice types, however using some of the discussed parameters, some differentiation can be accomplished.

Our results show that SAR data alone is not able to discriminate sea ice types during the melt season, however specific polarizations and incidence angles from Radarsat-2 data can assist in discrimination of FYI from MYI types during the melt season. Algorithms will need to make use of this information so as to be able to improve machine and human classification of Radarsat-2 data of this late season ice. Future on-ice work is required to understand the processes that govern the distribution of water in liquid phase within the MYI and FYI surface/volume. It is this distribution of water which dominates the microwave scattering at various incidence angles and polarizations and such knowledge of how and why water moves within MYI and FYI types will benefit their separability. Further work should also take into consideration the use of texture

analysis of the satellite imagery (e.g., Barber et al. 1998) taken at the polarizations (HH versus HV) and incidence angles (20°, 35° and 45°) investigated here. The use of texture analysis may be more appropriate for discriminating ice types (FYI versus MYI), and may further improve their identification in late melt season. The time series scattering over the diurnal cycling in summer may also provide a means of FY versus MY discrimination.

Acknowledgements

This research was supported through a Northern Studies Training Program grant to K. Warner, funding from Natural Science and Engineering Research Council of Canada (NSERC), Canada Research Chairs Program (CRC) and Centre for Earth Observation Science (CEOS) at the University of Manitoba. We would also like to thank Lauren Candlish, Ryan Galley, Monika Pucko, and the crew from the CCGS *Amundsen* for their help and contributions.

Literature Cited

Assur, A., and W.F. Weeks. 1982. "Growth, Structure and Strength of Sea Ice." *Cold Regions Research and Engineering Laboratory Monographs* 82 (1)

Barber, D. 2005. "Microwave Remote Sensing, Sea ice and Arctic Climate." *Canadian Journal of Physics* 61: 105-111.

Barber, D.G.; Fung, A.K.; Grenfell, T.C.; Nghiem, S.V.; Onstott, R.G.; Lytle, V.I.; Perovich, D.K.; Gow, A.J. 1998. The role of snow on microwave emission and scattering over first-year sea ice. Geoscience and Remote Sensing, IEEE Transactions. Vol. 36. No.5. Pp.1750-1763. Doi: 10.1109/36.718643

Barber, D., R. Galley, M. Asplin, R. De Abreu, K. Warner, M. Pucko, M. Gupta, S. Prinsenberg, and S. Julien. 2009. "The Summer perennial pack ice in the southern Beaufort Sea was not as it appeared to in the summer 2009." *Geophysical Research Letters* 36 (L24601) doi: 10.1029/2009GL041434

Carsey, F. (Ed.) 1992. *Microwave Remote Sensing of Sea Ice.* Geophysical Monograph Series. Vol. 68. 462 pp. AGU, Washington, D. C.

Comiso, J., C. Parkinson, R. Gersten, and L. Stock. 2008. "Accelerated decline in the Arctic Sea Ice Cover." *Geophysical Research Letters* 35 (L01703). doi: 10.1029/2007GL031972.

Covey, C., K, Taylor, and R. Dickinson. 1991. "Upper Limit for Sea Ice Albedo Feedback Contribution to Global Warming." *Journal of Geophysical Research* 96 (D5): 9169-9174. doi: 10.1029/91JD00236

Curry, J., J. Schramm, and E. Ebert. 1994. "Sea Ice-Albedo Climate Feedback Mechanism." *Journal of Climate* 8 (2). Pp. 240-247. Doi: 10.1175/1520-0442(1995)008<0240:SIACFM>2.0.CO;2

DeAbreu, R., J. Yackel, D. Barber, and M. Arkett. 2001. "Operational Satellite Sensing of Arctic First Year Sea Ice Melt." *Canadian Journal of Remote Sensing* 27 (5): 487-501.

Drinkwater, M. R., R. Kwok, D. P. Winebrenner, and E. Rignot. 1991. "Multifrequency Polarimetric Synthetic Aperture Radar Observations of Sea Ice." *Journal of Geophysical Research* 96 (C11): 679- 698. Doi:10.1029/91JC01915.

Eicken, H., T. C. Grenfell, D. K. Perovich, J. A. Richter-Menge, and K. Frey. 2004. Hydraulic controls on summer Arctic pack ice albedo, J. Geophys. Res., 109, C08007, doi:10.1029/2003JC001989.

Eicken, H., M. Lensu, M. Lepparanta, W. B. Tucker III, A. J. Gow, and O. Salmela 1995. Thickness, structure, and properties of level summer multiyear ice in the Eurasian sector of the Arctic Ocean, J. Geophys. Res., 100(C11), 22,697–22,710, doi:10.1029/95JC02188.

Golden, K.M. 2001. "Brine percolation and the transport properties of sea ice." *Annals of Glaciology* 33 (1): 28-36

Hilmer, M. and P. Lemke. 2000. "On the decrease of Arctic sea ice volume." *Geophysical Research Letters* 27 (22) 3751–3754. Doi: 10.1029/2000GL011403

Howell, S., and J. Yackel. 2004. "A vessel transit assessment of sea ice variability in the Western Arctic, 1969–2002: Implications for ship navigation." *Canadian Journal for Remote Sensing* 30 (2): 205-215

Isleifson, D., B. Hwang, D. Barber, R. Scharien, and L. Shafai. 2010. "C-Band Polarimetric Backscattering Signatures of Newly Formed Sea Ice During the Fall Freeze Up*." IEEE Transactions on Geoscience and Remote Sensing* 48 (8): 3256-3267.

Isleifson, D., A. Langlois, D. Barber, and L. Shafai. 2009. "C-Band Scatterometer Measurements of Multiyear Sea Ice Before Fall Freeze-Up in the Canadian Arctic." *IEEE Transactions on Geoscience and Remote Sensing* 47 (6): 1651-1661.

Johannessen, O. M., E.V. Shalina, and M.W. Miles. 1999. "Satellite evidence for an Arctic sea ice coverage in transformation." *Science* 286 (5446): 1937–1939. Doi: 10.1126/science.286.5446.1937

Kerr, R. 2002. "A warmer Arctic Means Change for All." *Science* 297 (5586): 1490-1493. doi: 10.1126/science.297.5586.1490

Kwok, R., E. Rignot, and B. Holt. 1992. "Identification of Sea ice Types in Spaceborne Synthetic Aperture Radar Data." *Journal of Geophysical Research* 97 (C2): 2391-2402. doi:10.1029/91JC02652

Kwok, R., G.F Cunningham, M. Wensnahan, I. Rigor, H.J. Swally, and D. Yi. 2009. "Thinning and volume loss of the Arctic Ocean Sea Ice Cover: 2003-2008. *Journal of Geophysical Research* 114 (C07005). doi:10.1029/2009JC005312

Laine, V. 2004. "Arctic sea ice regional albedo variability and trends, 1982–1998." *Journal of Geophysical Research* 109 (C06027) doi:10.1029/2003JC001818

Livingstone. C.E.; R.K. Hawkins, A.L. Gray, L. Drapier, L.D. Arsenault, K. Okamoto, T.L. Wilkinson, and D. Pearson. 1983. "The CCRS/Sursat Active-Passive

Experiment 1978-1980: the Microwave Signatures of Sea Ice." Canada Centre for Remote Sensing. Ottawa, Ontario, Canada.

Livingstone, C.E. 1991. "Springtime C-band SAR backscatter signatures of Labrador Sea marginal ice: measurements versus modeling predictions." *IEEE Transactions on Geoscience and Remote Sensing* 29 (1): 29-41. doi: 10.1109/36.103290

Mysak, L. and S. Venegas. 1998. "Decadal climate oscillations in the Arctic: A new feedback loop for atmosphere-ice-ocean interactions." *Geophysical Research Letters* 25 (19): 3607-3610. doi:10.1029/98GL02782

Nghiem, S.V. and C. Bertoia. 2001. "Study of multi-polarization C-band backscatter signatures for Arctic sea ice mapping with future satellite SAR: Ice and Icebergs." *Canadian Journal of Remote Sensing* 27 (5): 387-402.

Onstott, R., R. Moore, and W. Weeks. 1979. "Surface Based Scatterometer Results of Arctic Sea Ice." *IEEE Transactions on Geoscience Electronics* 17 (3): 78-85

Onstott, R.G.; Y.S. Kim, and R.K. 1984. "Active Microwave Measurements of Sea Ice Under Fall Conditions: The Radarsat/FIREEX Fa ll Experiment." Technical Report 331-30/578 – Final. University of Kansas Remote Sensing Laboratory, Lawrence, Kansas.

Onstott, R.G. and S. Gogineni. 1985. "Active Microwave measurements of Arctic Sea Ice under summer conditions." *Journal of Geophysical Research* 90 (C3): 5035-5044. Doi: 10.1029/JC090iC03p05035

Onstott, R. G., T.C. Grenfell, C. Matzler, C.A. Luther, and E.A. Svendsen. 1987. "Evolution of the microwave sea ice signatures during early summer and midsummer in the marginal ice zone." *Journal of Geophysical Research* 92 (C7): 6825-6835. doi:10.1029/JC092iC07p06825

Onstott, R. and R. Shuchman. 2004. "Chapter 3: SAR Measurements of Sea Ice *from* Synthetic Aperture Radar Marine Users Manual." National Oceanic and Atmospheric Administration (NOAA). Washington, DC.

Parashar, S. K. 1974. "Investigation of Radar Discrimination of Sea Ice." Ph.D. Dissertation. CRES Technical Report 185-13. University of Kansas Center for Research, Inc., Lawrence, Kansas,

Prinsenberg, S.J., I.K. Peterson, and S. Holladay. 1996. "Comparison of airborne electromagnetic ice thickness data with NOAA/AVHRR and ERS-1/SAR images." *Atmosphere-Ocean* 34 (1). Doi: 10.1080/07055900.1996.9649562.

Rampal, P., J. Weiss, and D. Marsan. 2009. “Positive trend in the mean speed and deformation rate of Arctic sea ice, 1979–2007.” *Journal of Geophysical Research* 114 (C05013). doi:10.1029/2008JC005066

Rigor, I., and J. Wallace. 2004. “Variations in the age of Arctic Sea-Ice and Summer Sea-Ice Extent.” *Geophysical Research Letters* 31 (L09401). doi:10.1029/2004GL019492

Rind, D., R. Healy, C. Parkinson, and D. Martinson. 1995. “The Role of Sea Ice in 2 X CO_2 Climate Model Sensitivity. Part 1: The Total Influence of Sea Ice Thickness and Extent.” *Journal of Climate*. Vol 8: 449-463. doi:10.1175/1520-0442(1995)008<0449:TROSII>2.0.CO;2.

Rothrock, D. A., Y. Yu, and G. A. Maykut. 1999. “Thinning of the Arctic sea-ice cover.” *Geophysical Research Letters* 26 (23): 3469-3472. doi:10.1029/1999GL010863.

Serrez, M., M. Holland, and J. Stroeve. 2007. “Perspectives on the Arctic’s Shrinking Sea-Ice Cover.” *Science* 315 (5818): 1533-1536. Doi: 10.1126/science.1139426

Scharien, R. K., T. Geldsetzer, D. G. Barber, J. J. Yackel, and A. Langlois. 2010. Physical, dielectric, and C band microwave scattering properties of first-year sea ice during advanced melt, J. Geophys. Res., 115, C12026, doi:10.1029/2010JC006257.

Soh, L.-K. 1999. “Texture Analysis of SAR sea ice imagery using gray level co-occurrence matrices.” *IEEE Transactions on Geoscience and Remote Sensing* 37 (2): 780-795

Stewart, E., S. Howell, D. Draper, J. Yackel, and A. Tivy. 2007 “Sea Ice in Canada's Arctic: Implications for Cruise Tourism.” *Arctic* 60 (4): 370-380.

Stofan, E.R. 1995. “Overview of result of Spacebourn Imaging Radar-C, X-Band Synthetic Aperture Radar (SIR-C/X-SAR).” *IEEE Transactions on Geoscience and Remote Sensing* 33 (4): 817-828

Thomas, D.N. and G.S. Dieckmann. 2010. “*Sea Ice:* Second Edition.” *Wiley-Blackwell Publishing*, Oxford, UK.

Washington, W., and G. Meehl. 1986. “General circulation model CO_2 sensitivity experiments: Snow-sea ice albedo parameterizations and globally averaged surface air temperature.” *Climatic Change* 8 (3): 231-141. Doi: 10.1007/BF00161596

Weeks, W. and S. Ackley. 1982. “The Growth, structure, and properties of Sea Ice.” *Cold Regions Research and Engineering Laboratory Monographs* 82 (1)

Wilson, K.J., J. Falkingham, H. Melling, and R. De Abreu. 2004. "Shipping in the Canadian Arctic: other possible climate change scenarios." *Proceedings of the Geoscience and Remote Sensing Symposium, 2004. IGARSS 2004. IEEE International* 3: 1853–1856. Doi: 10.1109/IGARSS.2004.1370699

Zwally, H. and P. Gloersen. 2008. "Arctic Sea Ice Surviving the Summer Melt: Interannual Variability and Decreasing Trend." *Journal of Glaciology* 54 (185): 279-296. Doi: http://dx.doi.org/10.3189/002214308784886108

CHAPTER FOUR: DIURNAL MEASUREMENTS OF C-BAND BACKSCATTER FROM MULTIYEAR ICE IN LATE MELT SEASON 2011

This paper has been prepared for submission and peer review to the *International Journal of Remote Sensing*. This work represents a chapter in my thesis that was conceived, analyzed and reported by myself as the senior author, with the co-authors contributions and help.

Warner, K.; Isleifson, D.; Scharien, R.; Komarov, A.; Landy, J. and D.G. Barber. Diurnal Measurements of C-band Backscatter From Multiyear Ice in Late Melt Season 2011. International Journal of Remote Sensing. (2012)

Abstract

The summer season is the highest traffic season throughout the Arctic, thus an understanding of ice signatures from satellite data is extremely important. The diurnal temperature fluctuations in summer result in variable multiyear ice (MYI) signatures, making it difficult to identify. In this paper, we investigate the effects of small diurnal temperature changes (typically less than 3°C) on the *in situ* C-Band scatterometer signatures of sea ice. Temperature trends occurring over a diurnal period, and the C-Band Scatterometer signature response to temperature are analyzed. During the 2011 melt season, the MYI signatures demonstrated variability of 5 dB for temperature changes less than 1.5°C. The results from this analysis suggest an inverse relationship between temperature and summer MYI signatures. The results from this paper further show that increasing temperatures are causing changes in the microwave scattering signatures of sea ice during the advanced melt season, evident in a transition in signatures from volume to surface scattering. This change in scattering complicates the segmentation of MYI from first year ice (FYI), and thus the ability to determine where the major navigation threats are.

4.1 Introduction

Due to climate change and an accelerated loss in summertime sea ice extent, there has been considerable attention focused on the polar regions in recent years. Temperatures have been steadily increasing in the Western Canadian Arctic (Turner et al., 2007) causing a new icescape, with a reduction in both areal extent and thickness of multiyear ice (MYI) (Kwok et al., 2009; Comiso, 2002; Rigor & Wallace, 2004; Stroeve et al., 2007; Nghiem et al., 2007). The reduction of MYI is correlated with an increase in young, seasonal, highly saline first year ice (FYI), as well as increased open water during summer. This transformation affects the movement and fluxes of gas, mass, energy as well as the biological and physical processes within sea ice (Isleifson et al., 2009; Maykut, 1978; Maykut and Perovich, 1987) and has feedbacks to the global climate (Rothrock et al., 1999; Hilmer & Lemke, 2000). These changes underline the importance of monitoring and estimating ice types from satellite-based remote sensing, particularly in the summer period.

Due to the vastness of the Arctic and the expense of field campaigns, satellite remote sensing is a critical means by which to monitor large-scale changes. Microwave remote sensing plays an important role in understanding the changes in sea ice (Barber, 2005); however there are still challenges that remain in linking small-scale geophysical characteristics of the ice and their effects on the microwave signal as recorded in a satellite image, especially in the summer period. Near-surface remote sensing experiments are used to evaluate how local-scale atmospheric changes can affect the geophysics of the sea ice, while simultaneously, radar measurements are used to

characterize the electromagnetic response of the ice. These local scale measurements can then provide the basis for understanding the key geophysical properties of the sea ice seen at the larger scale (i.e. satellite imagery) and help determine if there are optimal parameters for ice floe identification. Furthermore, near-surface experiments, for example using a polarimetric C-Band scatterometer, provide detailed sea ice scattering information coupled with changes in ice physics over the diurnal cycle, whereas satellite imagery provides a single measurement in time.

A considerable amount of research has focused on signatures from a C-Band scatterometer as well as synthetic aperture radar (SAR) remote sensing of sea ice during fall and winter seasons (Carsey (Ed.) 1992: Chapter 2, Chapter 3 and Chapter 5); Soh, 1999; Drinkwater et al., 1991; Kwok et al., 1992; Isleifson et al., 2009; Isleifson et al., 2010; Livingstone, 1991; Nghiem & Bertoia, 2001; Stofan, 1995), as well as during the early spring period, when changes in scattering are linked to temperature and morphological changes in the snow cover overlying the sea ice (Drinkwater, 1989; Barber et al., 2001). Due to the difficulties in ice type identification in the late summer melt season (Barber et al., 2009; Warner et al., in review) and the difficulty of studying ice in this season, little research has been done on the summer MYI scattering signatures, or how small temperature changes affect the microwave scattering signatures obtained from MYI. There is a significant amount of variation in the microwave signatures obtained from MYI during the advanced melt season, and there needs to be further research to acknowledge how microwave signatures respond to local scale temperature changes. This paper will attempt to answer some of the questions that remain.

The overall objective for this paper is to investigate how local temperature changes affect the *in situ* C-band microwave scattering from summer MYI. This will be addressed by (1) establishing how temperature-induced changes affect the geophysical properties of sea ice and how these affect the backscattering signatures obtained from a polarimetric C-Band scatterometer, (2) determining if there is a combination of polarization and incidence angle that is best for melt detection, and (3) investigating temporal variability in backscattered signatures from Radarsat-2 data to determine if there is an optimal time of day for floe discrimination.

4.2 Background

The physical properties of sea ice are important for gaining an understanding of the age and type of ice, as well as being critical for interpreting microwave signatures. MYI has more than one year's growth (thickness over 2 m) and has distinct physical and electromagnetic characteristics compared to first year sea ice (Tucker et al., 1992). Due to the melt processes that occur, the surface of MYI has significantly less brine, making it near fresh, and is characterized by the presence of air inclusions. The surface of MYI is often characterized by changes in topography, with areas of rounded hummocks and ridges surrounding melt ponds, which can be either in liquid form or covered by a lens of fresh ice.

The thermodynamic state of sea ice governs the heat exchange processes that occur between the ocean, sea ice and atmosphere (Petrich & Eicken, 2010). During cold winter months the temperature gradient between ocean-sea ice-atmosphere (OSA) interface consistently remains below freezing point (<0°C); however, warm summer air temperatures (>0°C) and warm ocean waters present a vastly different temperature

gradient. During the late summer, melt occurs from both the top and the bottom of the sea ice, and thermodynamic phase changes substantially modify the physical properties of the ice. Moreover, during the summer season there is an increase in the amount of incoming solar radiation and the snow that accumulated over the winter begins to melt. As air temperatures increase above 0°C, further freshening of the ice surface occurs as the water in liquid phase flushes the brine downwards, through brine flushing and gravity drainage. The brine and air pockets expand with increasing temperatures until they eventually coalesce to form vertical brine channels.

Since sea ice is a heterogeneous mixture of individual components including ice, brine, solid salts and air bubbles (Ulaby et al., 1986), it is considered a thermodynamically and dynamically active medium. It is the combination of geophysical properties and the thermodynamic state of sea ice that determines the microwave propagation through the medium. Scattering from sea ice is a result of a combination of surface roughness and dielectric properties of those individual components. The dielectrics define the basic electrical property of a material and have effects on the amount of electromagnetic reflection, absorption and scattering that occurs within the medium. Understanding the dielectric constant of sea ice allows for a basis of knowledge about the physical properties of the sea ice (Morey et al., 1984). During the cold period, multiyear ice has a low dielectric loss when compared to first year ice, due to its low salinity, allowing microwaves to penetrate deeper and enhance the volume scattering contribution to the scattered radar signature (Sandven & Johannessen, 2006). During the summer season there are changes in the physical properties that complicate the scattering mechanisms of multiyear ice from radar.

The penetration depth of C-Band microwaves into MYI during the summer is variable and dependant on the conditions as well as the depth of the salinity layer. Since the surface of MYI is near fresh with a low brine volume, the microwave is able to penetrate through the surface of the ice when conditions are cold, into the top section of the ice with air inclusions, usually to depth of when the brine volume increases. Since the microwave is able to penetrate the surface when conditions are cold, the scattering that occurs within the top 20-30 cm of fresh MYI, meaning the signatures were a result of volume scattering (Hallikainen & Winebrenner, 1992). However, as temperatures warm and melt progresses, there is a higher presence of water in liquid phase that accumulates on the surface of the ice. This water in liquid phase causes a change in the backscattered signatures of MYI from volume to surface scattering (Hallikainen and Winebrenner 1992). During the early summer season, temperatures are hovering close to freezing, therefore the signatures respond to small variations in temperature. Carlström and Ulander (1993) and Carlström (1995) found that when temperatures decreased the average backscattering signatures increased during the melt season. This variability in the scattering has been attributed to an increase in the penetration depth and more volume scattering.

4.3 Study Area and Methods

In situ data collection on sea ice geophysical properties was conducted northwest of Banks Island in the Beaufort Sea in the western Canadian Arctic (Figure 4.1), as part of a multidisciplinary research cruise aboard the CCGS *Amundsen*. The data used in this study were derived from the two multiyear ice stations that were sampled on 15 and 18 August 2011, named Site 1 (S1) and Site 2 (S2) respectively (Figure 4.1). Each site was

physically sampled (PS) four times (PS1-PS4). Upon arrival at a sampling station, the ship was moored to the side of the ice floe, thereby eliminating any relative drift between the vessel and the floe of interest.

Table 4.1: Details (date, time, location) on the sampled stations

Station Name	Latitude	Longitude	*In Situ* Physical sample name	Date (2011)	Time (local ship time)
S1	74.8556	-128.303	PS-1	15 August	9:53
			PS-2	15 August	14:00
			PS-3	15 August	21:50
			PS-4	16 August	8:30
S2	75.0277	-128.977	PS-1	17 August	13:30
			PS-2	17 August	19:50
			PS-3	18 August	9:10
			PS-4	18 August	15:40

At each station, ice physical property data were obtained at 6-hour intervals throughout the diurnal period; resulting in four data sets at each station (Table 4.1). Site photos were taken to accompany the qualitative observations of the surface conditions. Air temperature was measured by holding a hand-held temperature probe (Traceable® Digital Thermometer, Control Company, accuracy ±0.05 °C) approximately 1 m above the ice surface. The ice surface temperature was measured by placing the temperature probe in contact with the top of the ice floe. Ice cores were collected (using a 1m Kovacs Mark II coring system) in order to characterize the ice geophysics and thermodynamics. Temperature profiles were measured from a core immediately after extraction by drilling a hole in the core at 10 cm intervals and inserting a temperature probe. The second core extracted was used to measure salinity; the core was cut into 10 cm sections, which were then brought on board the ship to be melted in plastic buckets. Once melted, the salinity measurements were obtained using the conductivity and temperature readings from a HACH SENSION5, a portable conductivity meter, with an accuracy of +/- 0.01 PSU.

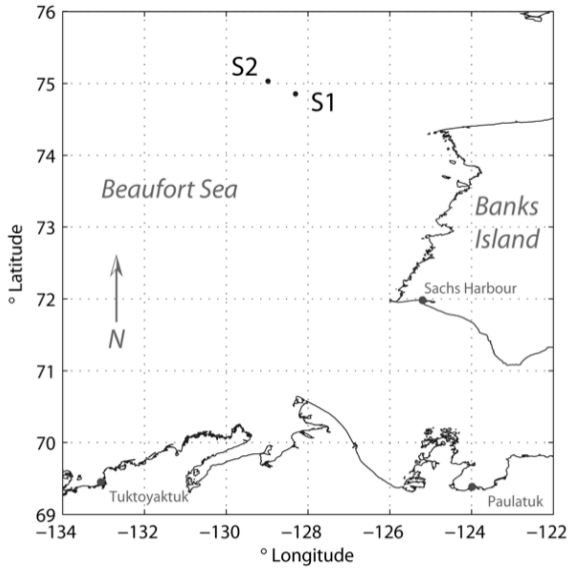

Figure 4.1: Area map showing in situ physical sampling stations

A C-band polarimetric scatterometer was used to measure backscatter from the sea ice at discrete time intervals corresponding to when the physical sampling measurements took place. The instrument was mounted on the port side of the ship at a height of 8 m with respect to the surface of the water. The system operates with a center frequency of 5.5 GHz and a bandwidth of 500 MHz. The antenna was a dual-polarized reflector with a beam width of approximately 5.5° in both the V-plane and H-plane. Measurements were conducted with 40° swaths in azimuth. Incident angles were set at 20° to 60° from nadir in discrete increments of 5°. The returned power was measured, and the covariance matrix was calculated allowing the VV, HV, and HH normalized radar cross sections (NRCS) to be obtained. At station S1 we obtained a calibration of the radar system using a trihedral corner reflector following the calibration method of Geldsetzer et al., (2007). This system has been used in various field campaigns and its

utility and processing have been discussed in Geldsetzer et al. (2007) and Isleifson et al. (2010).

At the first station, S1 (Figure 4.2a), backscattering data at the 25°, 45° and 60° incident angles were obtained. In S1, the 25° represents a near range ice surface signature, the 45° incident angle represents a melt pond, and the 60° represents a far range ice surface signature. At other incident angles, mixtures of surface types preclude their analysis within the context of the objectives of this study. At the second station, S2 (Figure 4.2b), data at incident angles 55° and 60° were chosen, and near range data were discarded due to the presence of open water and brash ice between the *Amundsen* vessel and the floe.

A. S-1

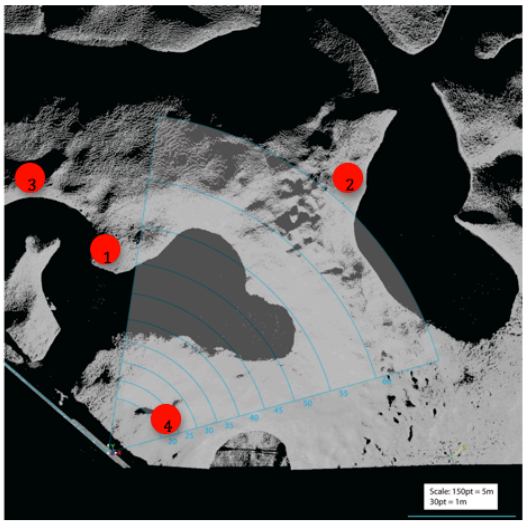

B. S-2

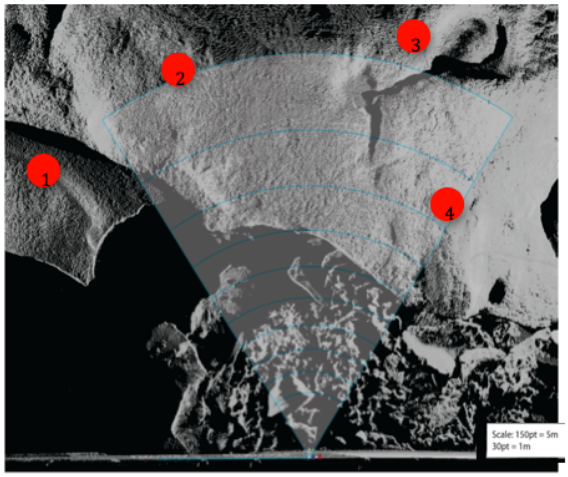

Figure 4.2: Study footprint from the scatterometer's view for A. S1 (sampled PS-) on August 15 2011 and B. S2 (sampled PS-) on August 17, 2011

Meteorological conditions were monitored using an automated weather station located on the bow of the *Amundsen*, at a height of approximately 14 m above the sea surface. Temperature measurements (one minute averages) from the weather station provide data for the complete diurnal cycle above the OSA, whereas *in situ* measurements obtained during sampling provide near-surface characterization.

Two standard product Radarsat-2 images were acquired for the sampling period. Radarsat-2 is a C-Band active microwave sensor that can be used to examine sea ice characteristics. The sensor operates at 5.3 GHz within the microwave band of the electromagnetic spectrum and has a wavelength of approximately 5 cm, allowing penetration depths from 0 cm (surface scattering) when conditions are wet up to about 30 cm (absorption with volume scattering) when conditions are dry (Onstott and Shuchman 2004; Barber 2005) in sea ice. The swath width from ScanSAR Wide product (Radarsat-2) is 500 km and has a spatial resolution of 50 m. This sensor also provides that option of obtaining data in single, dual or quad polarizations. These images were acquired on 13 and 17 August 2011. The image on 13 August represented a descending evening pass; while the 17 August was obtained during an ascending morning pass. These images were chosen because the incidence angles were similar enough to allow for comparison. Regions of interest (ROIs) were selected and exported from the satellite data for S1 and S2. Sigma naught (σ°) statistics (mean, standard deviation, minimum and maximum) of the ROIs were extracted. Sigma naught values are a conventional measure of the strength of radar signals reflected by the distributed scatterer, and are measured in decibels (dB).

4.4 Results and Discussion

4.4.1 Station S1

The physical property data collected at S1 indicate representative MYI, with a mean floe thickness measured at 4.3 m. There were changes in topography, such as low-lying areas with melt ponds, and areas of higher elevation, such as hummocks. It was late in the melt season, so there was no snow on the surface and the upper layer consisted of disaggregated ice.

A typical diurnal temperature cycle was observed at S1, which included a gradual warming throughout the day, peaking around 21:00 local time then cooling over night (Figure 4.3a). During the first sampling period on 15 August around 8:00 local time, PS1, temperatures from the tower were -1.25°C and the near-surface air temperature was -0.39°C. During this time, there was consistent cloud cover and high humidity. The melt ponds that were present remained frozen throughout and the surface of the ice remained dry. Into the afternoon, the air temperatures increased up to -0.9°C, and 1.2°C measured from the ice surface and conditions were consistent with those at the PS1 site. At PS3, the air temperature measured from the surface of the ice was 0°C, the cloud cover had dissipated and the surface of the ice began showing signs of melt. Air temperatures peaked between 17:00 and 23:00 local time with a maximum of 0.21°C and a minimum of -0.47°C. Air temperatures decreased during the night to -1.14°C around 5:00 local ship time on 16 August. During the final sampling session, PS4, the on ice air temperature measurement made at 8:00 local ship time was -1.64°C and there was a thin ice layer present on the melt ponds and the surface of the ice remained dry throughout.

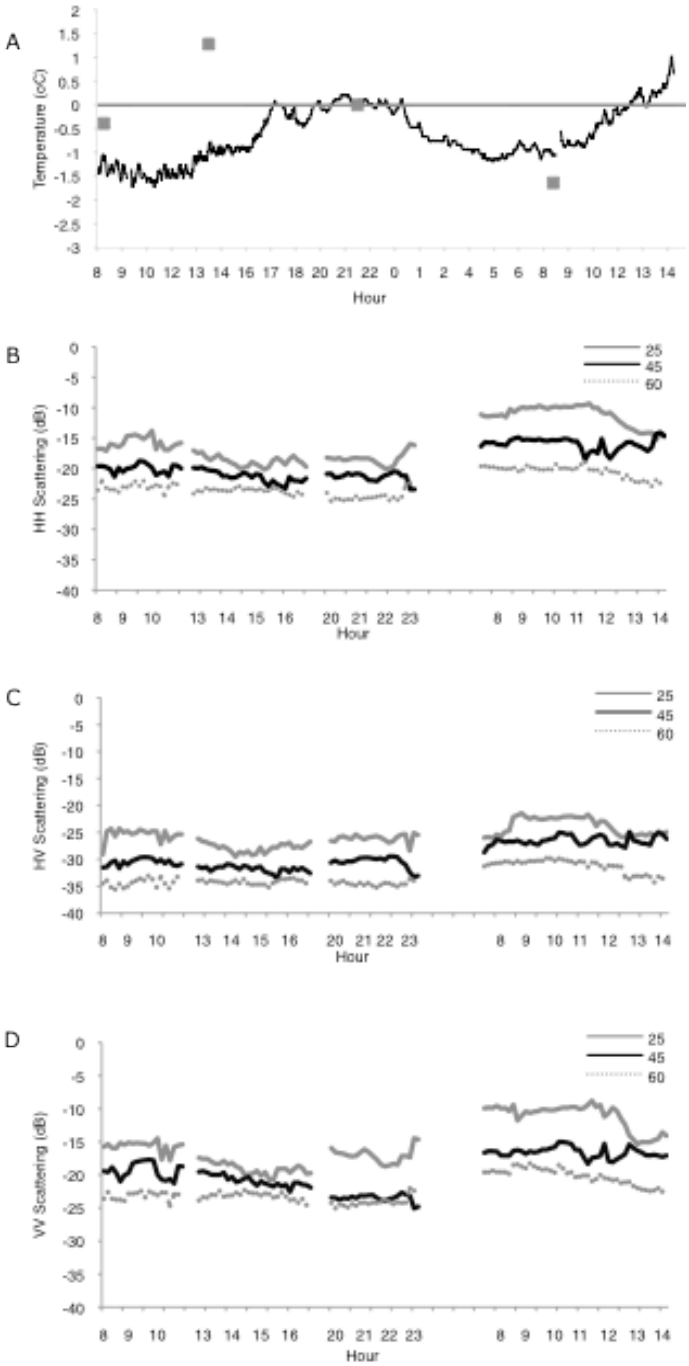

Figure 4.3: The diurnal cycling seen in various parameters at station S1 of (A) air temperature (on ice air temperature shown as points), (B) HH backscattering signatures, (C) HV backscattering signatures, and (D) VV backscattering signatures from sampling dates of 15 August to 16 August 2011.

Ice core temperatures from S1 are shown in Figure 4a. The temperatures at the first three sample locations (PS1, PS2 and PS3) were all between -1°C and 0°C within the top 40 cm. However, the last profile taken (PS4) shows the top 20 cm of the ice to be much colder and gradually warming until a depth of 25 cm.

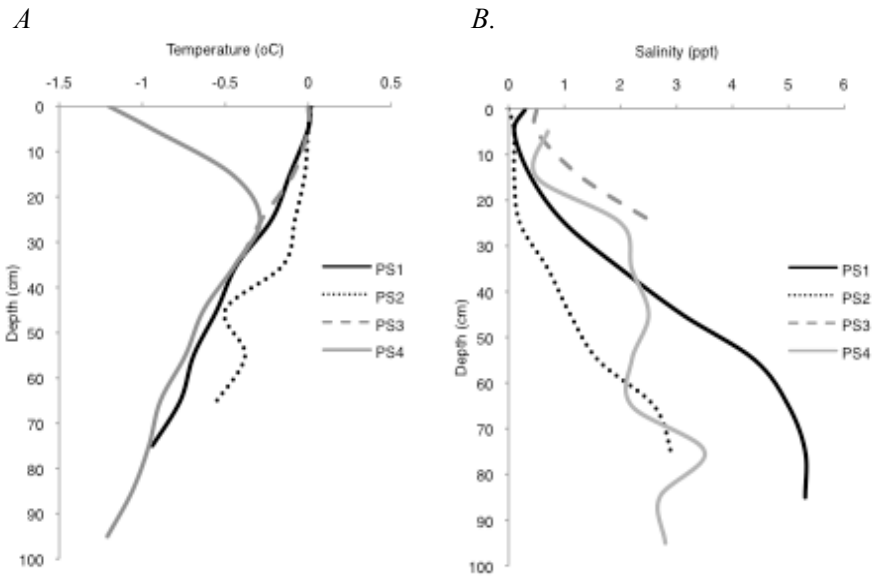

Figure 4.4: Temperature profiles (A) and salinity profiles (B) for multiyear ice station S1 sampled during 15 August to 16 August 2011.

The temperature variations observed while on station S1 (Figure 4.3a) can be associated with changes observed in C-band backscattering signatures. The mean scattering signatures obtained from each of the physical sampling stations (PS1-PS4) from S1 inversely follow the temperature trend (Figure 4.3). In the co-polarization signatures, there was large amount of variation in the backscattering signatures in response to the temperature variability (Table 4.2). The mean HH co-polarization signatures initially decreased during the first two scans (PS1-PS2) when temperatures were consistently below 0°C; however, the signatures measured during PS4 were, on

average, significantly higher (Figure 4.3b). During the time spent at S1, the mean HH signatures from the 25°, 45° and 60° incident angles increased by 4.5 dB, 4 dB and 2.4 dB respectively (Table 4.2). The mean VV co-polarized signatures followed a very similar pattern seen in the co-polarized HH signatures (Figure 4.3d and Table 4.2). The mean signatures from the 25°, 45° and 60° incident angles increased by 4.5 dB, 2.7 dB and 2.9 dB respectively throughout the 28 hours spent at S1. Overall, the cross-polarized signatures showed less variation between sites [seen in the backscattering signatures], however still followed the temperature trend. During PS1, the signatures were generally stable as temperature remained below 0°C (Figure 4.3d). During PS2, there was a small decrease in scattering as temperatures increased and then once again at PS4, the signatures were on average higher (Figure 4.3c), which coincided with a cooler temperature. The mean signatures from the 25°, 45° and 60° incident angles increased by 1.5 dB, 4 dB and 3 dB respectively throughout the 28 hours spent at S1 (Table 4.2).

Table 4.2: Statistics (maximum, minimum and mean) for each sampling site S1 in each of the polarizations (HH, HV and VV) at the various incident angles.

				HH			**HV**			**VV**		
STN Name	**Sample Site**	**Temp (°C)**	**Inc ∠ (°)**	Max (dB)	Min (dB)	Mean (dB)	Max (dB)	Min (dB)	Mean (dB)	Max (dB)	Min (dB)	Mean (dB)
S1	PS1	-1.41	25	-13.8	-17.1	-15.8	-24.3	-29.1	-25.3	-14.5	-17.8	-15.6
			45	-18.7	-21.3	-19.9	-29.6	-31.7	-30.5	-17.7	-21.3	-19.3
			60	-22.0	-24.4	-22.9	-33.1	-35.6	-34.3	-22.5	-24.7	-23.1
	PS2	-0.94	25	-17.0	-20.2	-18.8	-26.2	-29.5	-27.8	-17.4	-20.8	-19.0
			45	-19.8	-23.3	-21.3	-30.9	-33.6	-31.8	-19.4	-22.6	-20.9
			60	-22.9	-24.6	-23.7	-33.5	-35.1	-34.2	-22.3	-24.6	-23.2
	PS3	0.03	25	-15.9	-20.0	-18.4	-25.1	-28.4	-26.1	-14.5	-18.7	-17.0
			45	-20.5	-23.4	-21.4	-29.5	-33.3	-30.5	-22.7	-25.1	-23.5
			60	-22.4	-25.4	-24.5	-33.7	-35.2	-34.5	-22.0	-25.0	-24.1
	PS4	-0.29	25	-9.3	-15.3	-11.3	-21.4	-26.1	-23.8	-8.8	-15.3	-11.1
			45	-14.0	-18.6	-15.9	-24.9	-28.7	-26.5	-15.0	-18.3	-16.6
			60	-18.9	-23.0	-20.5	-29.8	-34.3	-31.3	-18.3	-22.6	-20.2

There were periods where the air temperatures were consistently below 0°C and there was little variation; during this time there were virtually no changes in the ice

temperature and salinity profiles, and as a result the measured backscattering signatures responded accordingly and remained stable. It was not until the temperatures began to change that the backscattering signatures responded. In PS2, as temperatures began to increase above 0°C, it can be seen that signatures responded (Figure 4.3). The co-polarized (HH and VV) backscattering signatures (Figure 4.3b and 4.3d) measured at incident angles 25° and 60°, decreased, while the melt pond signature (45°) became increasingly variable. PS4 had cold temperatures at the beginning of the sampling period, but as time progressed the temperature increased above 0°C; when temperatures increased above 0°C around 12:00 local time, the backscattering responded and decreased almost immediately. This pattern was consistently observed, showing that an inverse relationship was observed between the temperature and the measured backscattering intensity. It may be possible that these inverse correlations between temperatures and backscattering signatures be computed and perhaps algorithms could be designed around these calculations.

The connection between *in situ* air temperature and backscattering was especially evident for PS4. The *in situ* air temperature measurement was -1.64°C, which was the coldest measurement obtained throughout the entire sampling period (Figure 4.3a). At this time, the temperature of the ice was -1.2°C, making it colder than all of the other ice core samples. In all of the backscattering signatures obtained from this time period, the signatures were higher in all incident angles and polarizations (Figure 4.3b, 4.3c, 4.3d).

Further analysis was done with the backscattering signatures obtained from the C-Band scatterometer investigating if there was a combination of incident angle and polarization that would be best for melt detection at this site. At S1, it became clear that

the largest difference between the signatures from the original state was seen in HH and VV co-polarization at smaller incident angle (25°); there were increases in the backscattering by 4.5 dB when temperatures fell below 0°C and decreases in the signatures by approximately 3 dB when temperatures increased above 0°C. There was less variation in the cross-polarization data even while temperatures rose and fell below 0°C at the incidence angles representing ice (25° and 60°). This analysis has shown that co-polarization data from smaller incidence angles would be best for detection of melt.

4.4.2 Station S2

The physical property data collected at S2 was on another multiyear ice flow, with a mean thickness of 3.6 m, but consisted of areas with ice as thick as 8 m and areas of ice as thin as 1 m; these variations were a result of interspersed hummocks and melt ponds. The sampling done at S2 occurred in the advanced melt season, and as a result, the snow that had been present on the surface of the ice had melted creating a bare ice surface.

Throughout the diurnal measurement period at S2, a very different temperature regime was seen when comparing with S1. During the time spent at this station, a stable near isothermal temperature was observed (Figure 4.5a). During the first sampling period there was a light cloud cover and temperatures were approximately -0.6°C (Figure 4.5a). During that first sampling period, the surface of the ice was dry with no evidence of melt. However, as time progressed, conditions became overcast and a light fog was present, and at approximately 20:00 the temperature rose above 0°C (Figure 4.5a). Once the temperature was above 0°C, the surface of the ice began to melt and became visibly wet. Temperatures continued to warm and during the last sampling session, PS4, it was still

overcast with intermittent light fog, however average tower temperature measurements had further warmed up to 0.47°C and the *in situ* air temperature was 0.4°C

All physical sampling at S2 was conducted from the surface of hummocks. Temperature profiles were consistent with one another (Figure 4.6a) and nearly isothermal, between -1°C and 0°C. The only difference was observed at PS3 (Figure 4.6a), when the ice temperature was colder between 65cm to 90cm, reaching a minimum of -1.5°C. The salinity profiles (Figure 4.6b) at this station were more variable than those in S1, however were typical of hummock ice on MYI. The surface of the ice was fresh with little to no salinity and around the 20 cm mark, the salinity profiles all become variable, alternating between low, 0.5 PSU, up to 3 PSU. All of the profiles are near-fresh at the surface, which is typical of MYI, and salinity concentration increased with depth.

The second sampling station, S2, exhibited notably different environmental conditions and as a result different backscattering signatures in comparison to S1. The lack of air temperature variation seen while at this station can be linked to relatively constant C-band backscatter signatures. The mean HH co-polarized backscatter decreased at approximately 14:00 local time, remained stable throughout PS2, PS3 and was followed by a decrease in PS4 (Figure 4.5b). The mean backscatter at 55° and 60° incident angles decreased by 4.6 dB and 2.6 dB respectively throughout the 26 hours spent on station (Table 4.3). The mean VV co-polarized signatures experienced similar trends as the HH signatures, including a general decrease over time. The measurements made from 55° and 60° incident angles decreased by 4.1 dB and 3.3 dB respectively throughout the 26 hours spent on station (Figure 4.5 and Table 4.3). The mean HV cross-polarized signatures saw significantly less variation over time, but still had an overall

trend showing a decrease in backscatter throughout the 26 hours spent on station. The only times showing variation throughout the sampling period occurred during PS1 around 14:00 and PS4 around 16:00 (Figure 4.5c). The mean HV signatures from 55° and 60° incident angles decreased by 0.9 dB and 1.9 dB respectively throughout the 26 hours spent on station (Figure 4.5c and Table 4.3).

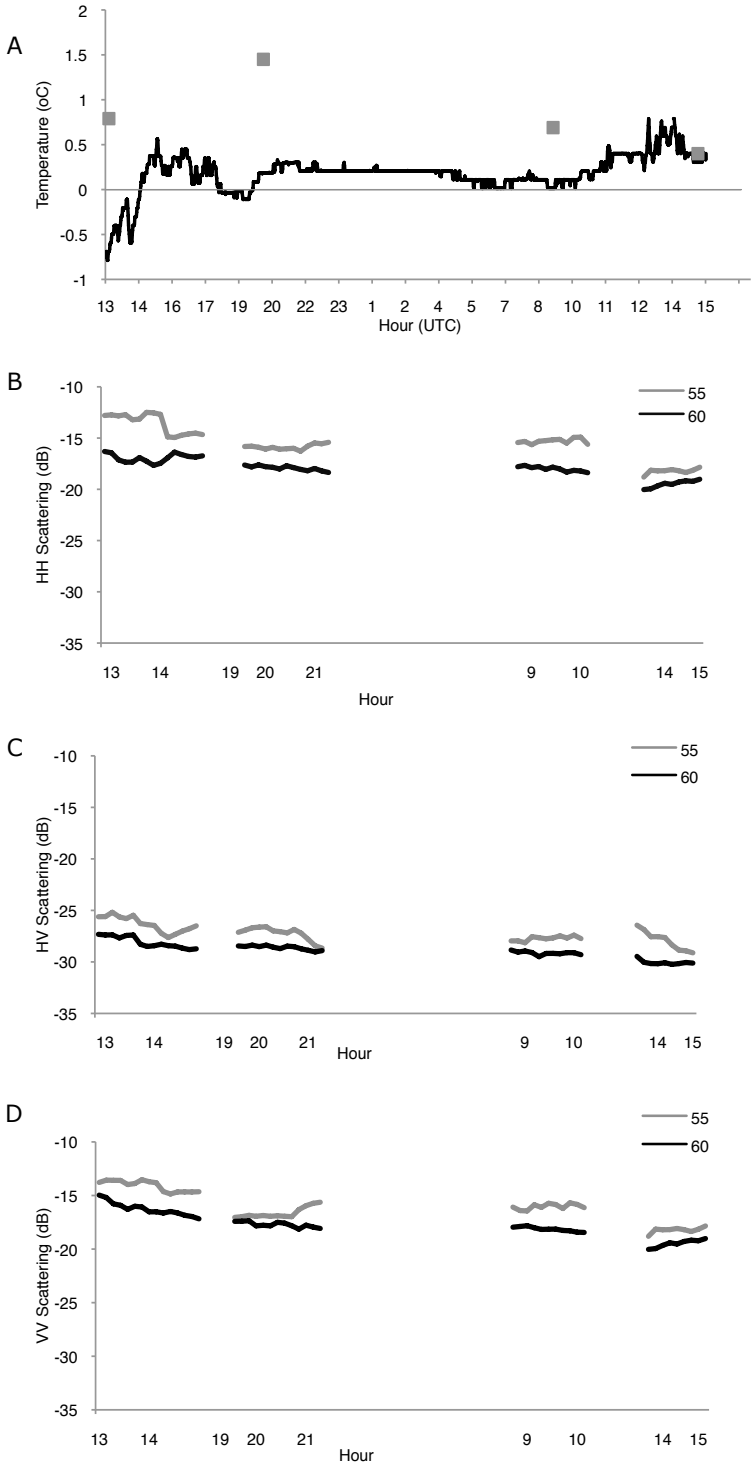

Figure 4.5: The diurnal cycling seen in various parameters at station S2 of (A) temperature, (B) HH backscattering signatures, (C) HV backscattering signatures, and (D) VV backscattering signatures from sampling dates of 17 August to 18 August 2011.

This sampling site was especially useful to understand how signatures respond to temperature changes, as there was little variation in the temperature. At the beginning of sampling, the increase in temperature that occurred caused increased melt and as a result, an increase in water in liquid phase present on the ice surface. Since temperature remained above 0°C for a majority of the sampling time, melt was constantly occurring. There were two points worth noting throughout S2 that show a relationship between temperature and the measured backscattering signatures. The first occurred during PS1 at 14:30 local ship time; there was a drop in backscattering signatures at this time, which coincides with the temperature rising above 0°C. As the temperature increased, the co-polarized signatures, both HH and VV decreased. The second point to take note of occurred in PS4. It can be seen throughout PS2 and PS3, the temperature is very stable, and as a result the backscattering is as well. However, PS4 had an increased temperature up to the warmest experienced, 0.789°C, which occurred at 14:00 local ship time (Figure 4.6a). When this increase in temperature occurred, the signature in both co-polarized signatures (HH and VV in Figure 4.6b and 4.6d respectively), were noticeably less than the average backscattering measurements made throughout the sampling period, confirming that there is an inverse relationship between temperature and scattering signatures. The overall trend that occurred while on station S2 was a decrease in backscatter intensity throughout the 26 hours spent on station.

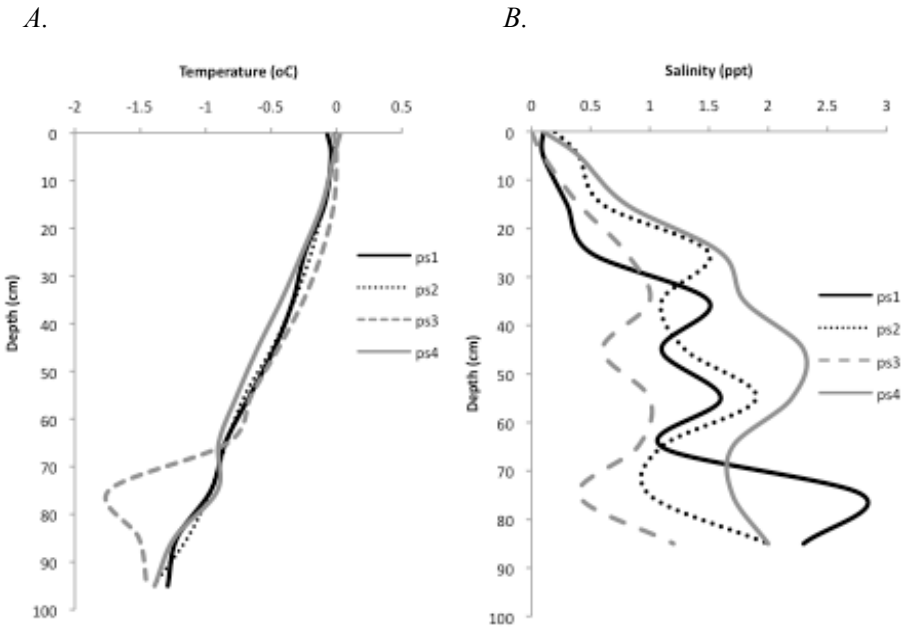

Figure 4.6: Temperature profiles (A) and salinity profiles (B) for multiyear ice station S2 sampled from dates of 17 August to 18 August 2011.

There was a further investigation done to determine if there was a combination of incident angle and polarization that would be best for melt detection at this site. Similar to the first sampling site, HH and VV co-polarization signatures from smaller incidence angles (55°) at S2 showed the greatest amount of change from their original state. At the 55° incidence angle, the HV cross-polarization data had a maximum decrease of 1.6 dB, while the HH co polarization signature decreased by 4.6 dB and the VV signature by 4.1 dB. The 60° incidence angle saw overall less variability as conditions were changing, ultimately showing that, once again, the co-polarized data at smaller incidence angles were better for melt detection.

Table 4.3: Statistics (maximum, minimum and mean) for each sampling site S2 in each of the polarizations (HH, HV and VV) at the various incident angles.

				HH			HV			VV		
STN Name	Sample Site	Temp (°C)	Inc ∠ (°)	Max (dB)	Min (dB)	Mean (dB)	Max (dB)	Min (dB)	Mean (dB)	Max (dB)	Min (dB)	Mean (dB)
S2	PS1	-0.08	55	-12.5	-14.9	-13.6	-25.1	-27.6	-26.3	-13.5	-14.9	-14.1
			60	-16.3	-17.7	-16.9	-27.3	-28.8	-28.1	-14.9	-17.1	-16.2
	PS2	0.2	55	-15.4	-16.3	-15.9	-26.6	-28.7	-27.2	-15.6	-17.0	-16.6
			60	-17.6	-18.3	-17.9	-28.4	-29.0	-28.6	-17.4	-18.1	-17.7
	PS3	011	55	-14.9	-15.6	-15.3	-27.4	-28.1	-27.7	-15.9	-16.4	-16.0
			60	-17.7	-18.4	-18.0	-28.8	-29.5	-29.1	-17.8	-18.4	-18.1
	PS4	0.48	55	-17.8	-28.8	-18.2	-26.4	-29.1	-27.9	-17.8	-18.8	-18.2
			60	-19.0	-20.0	-19.5	-29.5	-30.2	-30.1	-19.0	-20.0	-19.5

4.4.3 Discussion

It is evident from the data that the occurrence of small temperature changes (less than 3 degrees Celsius), including fluctuations above and below the freezing point, had a significant effect on the *in situ* C-band backscatter measurements. The large effects on backscattered signatures from the small temperature variations ultimately show the difficulty of accuracy of microwave data in the late summer season. The C-band scatterometer captured considerable amounts of variability in the backscattering signatures from MYI that were measured throughout the diurnal cycle. Most satellite sensors only have the ability to capture a snapshot or a moment in time, so the data collected from these sensors is highly dependent on when the satellite overpass occurs. This indicates a need for additional analysis to determine if an optimal time of day to collect data to classify ice conditions exists.

Significant differences exist between sampling sites S1 and S2. The first sampled site (S1) saw a natural diurnal variation in temperature, which caused variability in the backscattering signatures (Figure 4.3). The second sampled site (S2) was below 0°C at the beginning of the sampling period, but quickly warmed and remained above 0°C for the duration of time spent on station (Figure 4.5). Differences in temperature

measurements between the two stations create an ideal data set for investigating if and how small changes in the temperature affect the scattering signatures. The two sites were representative MYI floes and were physically similar to one another, with alternating topography due to the presence of hummocks and melt ponds.

An inverse relationship between air temperatures and the backscatter signatures was detected at both stations. It was expected and observed that when air temperatures were cold, the ice was cold and dry, allowing the microwave to penetrate into the ice, giving a volume scattering signature (Hallikainen and Winebrenner 1992), thus causing stronger backscattering signatures. However, when temperatures increased above 0°C the surface of the ice was subject to melt and a greater presence of water in liquid phase. A layer of liquid water on the surface is known to mask the underlying ice from the microwaves, meaning the scattering signatures weaken and reverse, becoming primarily surface scattering (Hallikainen and Winebrenner 1992). At S1, temperatures followed a more typical diurnal cycle, dropping below freezing during the night causing the liquid water to freeze, resulting in a volume scattering signature. During the mid-day, when the temperatures increased above zero, melt occurred at the surface of the ice, increasing the amount of scattering from the surface. These were seen from the signatures obtained from S1 (Figure 4.3); the measurements made in the morning, when temperatures were colder, were consistently higher, as they are likely a result of volume scattering. The signatures collected later in the afternoon when temperatures were warmer were, on average, lower indicating that more of the scattering was occurring from the surface and reflecting away. The second sampling station, S2, did not follow a diurnal temperature pattern; upon arrival temperatures were cold, but rapidly warmed above 0°C where they remained for

the duration of sampling. The highest backscattering signatures that were measured were obtained from that first sampling station, PS1, which coincided with the only measurement made when temperatures were still below 0°C. Otherwise, the backscattered signatures decreased over time as temperatures increased. At S2, the air temperatures were more stable, remaining above 0°C for a majority of the sampling. The stable temperatures caused that lack of variability seen in the signatures (Figure 4.5). Due to the warmer temperatures and a greater presence of water in liquid phase, it can be assumed that there was likely more of a surface scattering contribution to the backscattering signatures.

Investigation as to whether an optimal time of day for data collection exists using the *in situ* C-Band scatterometer data, taking the most similar times of day for each station, S1 and S2, and comparing the average backscattered values at the shared incidence angle of 60°, showed that mornings have the least amount of difference between values, with a difference of 4.9 dB in HH signatures, 5 dB in VV signatures and 5.2 in HV. As the day progressed temperatures warmed and the amount of incoming solar radiation increased, which led to further melt on the surface of the ice, and increased variability in the measured *in situ* signatures; differences between the evening HH signatures at S1 (PS3) and S2 (PS2) was 6.6 dB, 6.4 dB in VV signatures and 5.9 in HV signatures. This shows that the morning signatures, when temperatures are cooler and there is less incoming solar radiation, are more likely to be from a result of volume scattering. As the day progresses, temperatures increase, the amount of incoming solar radiation increases and surface melt occurs, causing the signatures to revert to surface scattering.

An analysis of these same sites, S1 and S2, was done using Radarsat-2 data to investigate if the differences in measured backscattered signatures between morning and evening also existed at larger spatial scales. This analysis took two data products, one from 13 August 2011 represents a descending evening pass and the other from 17 August 2011 represents an ascending morning pass for comparison. The difference between incidence angles for the two images was less than 5°, making them ideal for comparing the differences brought on by the time of day. The analysis included the extraction of multiple regions of interest (ROI's) from S1 and S2. It is interesting to note that the morning overpass (20110817) had consistently higher backscattered signatures when compared to the evening pass (20110813). At S1, the morning overpass signatures were on average 3.3 dB to 5.2 dB higher than the evening backscattering signatures (Table 4.4). At S2, the morning overpass signatures were, once again, on average 1.7 dB to 4.8 dB higher than the evening pass (Table 4.4). The consistently higher measured backscattered signatures from the morning overpass show that it is likely that there is more scattering occurring from the volume at this time, and as the day progresses there are lower measured backscattered signatures, *symbolizing a transition to surface scattering.*

Table 4.4: Mean backscattered Sigma naught (σ^o) values obtained from Radarsat-2 data (measured in dB)

S1				
Date	**ROI_1**	**ROI_2**	**ROI_3**	**ROI_4**
20110813	-20.51	-18.72	-19.19	-18.8
20110817	-15.31	-15.11	-14.5	-15.54
S2				
20110813	-19.42	-17.69	-18.59	-19.94
20110817	-15.33	-16.03	-15.92	-15.16

It has been shown that diurnal changes in temperature have affects on the microwave scattering signatures obtained. This study found that when the temperatures were variable at S1 (Figure 4.3a) there were changes as high as 4.5 dB in the HH co-polarized signatures of near range MYI (25° incident angle) (Figure 4.3b and Table 4.2). Nghiem et al. (1997) saw similar results when conducting a study of the diurnal thermal cycles and their effects on microwave signatures in a controlled environment of thin perennial sea ice. They observed that diurnal variations in temperature caused changes as high as 6 dB in the signatures obtained from a C-Band scatterometer, and saw that the diurnal cycles in temperature can also cause the dominant scattering mechanisms to reverse. Livingstone et al. (1987) also showed that there were larger variations in the signatures obtained from an aircraft mounted Ku-Band scatterometer of both FYI and MYI during the melt season than during any other season. Barber et al. (1992a) investigated microwave scattering signatures from synthetic aperture radar (SAR) data from Sea ice and Terrain Assessment Radar-2 (STAR-2) of MYI and FYI both spatially and temporally, and similar to the other studies mentioned, saw that the geophysical properties of multiyear sea ice created a large and rapid change in the scattering signatures during the melt season. It was noted that multiyear ice is sensitive to the seasonal transition and as a result, the geophysical properties of the ice are altered, which ultimately change the backscattering. Furthermore, Barber et al. (1992b) conducted a study that included an analysis of scatterometer data, modeling data, and image data that saw that as temperatures increased, there was a decrease in volume scattering and an increase in surface scattering in fast ice, meaning a decrease in the backscattering signatures. Livingstone and Drinkwater (1991) also showed results that has scattering

signatures reversing when temperatures increase and water in liquid phase increases, with measurements occurring at melt onset in spring with SAR backscattered signatures of marginal ice.

4.5 Conclusions

The overall objective of this paper was to explore how small temperature changes affect the *in situ* multiyear sea ice microwave signatures in the summer season. This was addressed by (1) establishing how temperature induced changes affect the geophysical properties of sea ice and how these changes affect the backscattering signatures obtained from a polarimetric C-Band scatterometer, (2) determining if there was a combination of polarization and incidence angle that was best for melt detection of multiyear sea ice, and (3) investigating the sites' temporal variability in backscattered signatures from Radarsat-2 data to determine if there is an optimal time of day for floe discrimination. The results obtained from this analysis add to pre-existing knowledge that multiyear ice signatures are especially difficult to characterize during the late melt season, when significant diurnal variations in temperature occur.

During that first sampling period, S1, temperatures were variable, rising above and falling below 0°C, and as a result signatures changed by approximately 3-4.5 dB during the observed diurnal cycle (Figure 4.3). During the second sampling period, S2, the major variability in temperature occurred during PS1 and PS4, when they were increasing (Figure 4.5). Throughout S2, signatures varied by approximately 3-4.5 dB. It is interesting to note that the temperature and backscattering signature trends were inversely associated. The difference in the microwave signatures from initial state was calculated to determine if there was an optimal combination of incidence angle and

polarization for melt detection. The differences were consistently larger at the smaller incidence angles (25° at S1 and 55° at S2), suggesting that co-polarized data (HH or VV) are better than cross-polarized data for detecting the physical changes in the ice during the melt season.

The analysis examined the backscattered signatures at larger spatial scales using satellite imagery in order to determine if there was an optimal time of day to discriminate MYI and FYI floes from the data. Using Radarsat-2 data, there was a comparison between a morning and an evening overpass. Spatially, these floes had little to no variability in signatures as they were both characteristic MY floes with very similar physical characteristics. Temporally, however, there were differences in signatures that were dependent on the time of acquisition. This analysis led to the discovery that morning overpasses had consistently higher backscattered values than the evening overpass. The changes in the scattering signatures can be attributed to what one would expect in a normal diurnal cycle; in the morning temperatures are cooler, therefore signatures would be attributed to volume scattering. As the day progressed and temperatures warmed, melt began to occur which caused a decrease in the backscattering signatures due to the presence of water in liquid phase causing surface scattering.

The results from this analysis show that microwave signatures are highly variable during the melt season. It was shown that small changes in temperature, such as rising from -0.5°C to above 0°C can cause changes in the C-Band scatterometer signatures on magnitudes of multiple decibels. It is the distribution of water in liquid phase that changes as the temperatures change. This layer of water blocks the microwave from penetrating into the multiyear ice and as a result, surface scattering occurs from the

multiyear ice surface, causing confusion with first year ice signatures. As traffic increases throughout the Arctic passages, it is becoming increasingly important to have knowledge on where the multiyear ice is, as it has the greatest threats associated with it.

The results from this paper are especially important as conditions change in the Arctic. With a new record low sea ice extent reached in August 2012 (NSIDC, 2012), there will be a higher presence of traffic through the Arctic. Currently, a majority of the satellites that monitor the Arctic have a small temporal resolution, only acquiring a maximum of two images per day; this analysis, however, has shown that morning overpasses are likely better for collecting data for ice classification.

Acknowledgements

This research was supported through a Northern Studies Training Program grant to K. Warner, funding from Natural Science and Engineering Research Council of Canada (NSERC), Canada Research Chairs Program (CRC) and Centre for Earth Observation Science (CEOS) at the University of Manitoba. We would like to thank the crew from the CCGS *Amundsen* for their help and contributions.

Literature Cited

Barber, D.G.; Flett, D.G.; De Abreu, R. A. and E. F. LeDrew. 1992 [1]. Spatial and Temporal Variation of Sea Ice Geophysical Properties and Microwave Remote Sensing Observations: The SIMS' 90 Experiment. Arctic. Vol. 45. No. 3. Pp. 233-251

Barber, D.G.; LeDrew, E.F.; Flett, D.G.; Shokr, M. and J. Falkingham. 1992 [2]. Seasonal and Diurnal Variations in SAR Signatures of Landfast Sea Ice. IEEE Transactions on Geoscience and Remote Sensing. Vol. 30. No. 3. Pp. 638-642. Doi: 0196-2892/92

Barber, D.G. 2005. Microwave Remote Sensing, sea ice and Arctic climate. Canadian Journal of Physics. Vol. 61. Pp.105-111.

Barber, D.G.; Marsden, R.; Minnett, P.; Ingram, G.; and L. Fortier. 2001. Physical processes within the North Water (NOW) Polynya. Atmosphere Ocean. Vol. 39. Pp. 163–166.

Barber, D.G.; Galley, R.; Asplin, M.; De Abreu, R.; Warner, K.; Pucko, M.; Gupta, M.; Prinsenberg, S.; Julien, S. 2009. The Summer perennial pack ice in the southern Beaufort Sea was not as it appeared to in the summer 2009. Geophysical Research Letters. Vol. 36. No. 24.

Carlstrom, A. 1995. Modeling microwave backscattering from sea ice for synthetic aperture radar applications. School of Electrical and Computer Engineering, Chalmers University of Technology, Goteborg, Sweden. Technical Report 271.

Carlstrom, A.; and Lars M.H. Ulander. 1993. "C-Band Backscatter Signatures of Old Sea Ice in the Central Arctic During Freeze-Up." *IEEE Transactions on Geoscience and Remote Sensing.* Vol. 31. Pp. 819-829.

Carsey, F. (Ed.) 1992. Microwave Remote Sensing of Sea Ice. Geophys. Monogr. *Ser.*, vol. 68, 462 pp., AGU, Washington, D. C.

Comiso, J.C. 2002. “A Rapidly declining sea ice cover in the Arctic. Geophysical Research Letters. Vol. 29. No. 20. DOI: 10.1029/2002GL015650

Drinkwater, M.R. 1989. LIMEX’87 Ice surface characteristics; implications for C-Band SAR backscatter signatures. IEEE Transactions on Geoscience and Remote Sensing. Vol. 27. No. 5. Pp. 601-613

Drinkwater, M.R. and G.B. Crocker. 1988. Modeling changes in the dielectric and scattering properties of young snow covered sea ice at GHz frequencies. Journal of Glaciology. Vol. 34. No. 118. Pp. 274-282.

Geldsetzer, T.; Mead, J.B.; Yackel, J.J.; Scharien, R.K. and S. E. L. Howell. 2007. Surface-based polarimetric C-band scatterometer for field measurements of sea ice, IEEE Transactions on Geoscience and Remote Sensing. Vol. 45. No. 11. Pp. 3405-3416, doi:10.1109/TGRS.2007.907043

Hallikainen and Winebrenner 1992. Microwave Remote Sensing of Sea Ice. American Geophysical Union. Vol. 68. Chapter 3: The Physical Basis for Sea ice Remote Sensing

Hilmer, M. and Lemke, P. 2000. On the decrease of Arctic sea ice volume. Geophysical Research Letters. Vol. 27. No. 3751–3754.

Isleifson, D.; Hwang, B.; Barber, D.; Scharien, R.; Shafai, L. 2010. C-Band Polarimetric Backscattering Signatures of Newly Formed Sea Ice During the Fall Freeze Up. IEEE Transactions on Geoscience and Remote Sensing. Vol. 48. No. 8. pp. 3256-3267.

Isleifson, D.; Langlois, A.; Barber, D.; Shafai, L. 2009. C-Band Scatterometer Measurements of Multiyear Sea Ice Before Fall Freeze-Up in the Canadian Arctic. IEEE Transactions on Geoscience and Remote Sensing. Vol. 47. No. 6. pp. 1651-1661.

Kwok, R., Rignot, E., Holt, B. 1992. Identification of Sea ice Types in Spaceborne / Synthetic Aperture Radar Data. Journal of Geophysical Research. Vol. 97. No. C2. Pp. 2391-2402

Kwok ,G.F.; Cunningham, M.; Wensnahan, I.; Rigor, H.; Zwally, J.; Yi, D. 2009. Thinning and volume loss of the Arctic Ocean Sea ice Cover: 2003-2008. Journal of Geophysical Research. Vol. 114. No. C7. Pp. C07 005. DOI: 10.1029/2009JC005312.

Livingstone, C.E.; Singh, K.P. and A. L. Gray. 1987. Season and Regional Variations of Active/Passive Microwave Signatures of Sea Ice. IEEE Transactions on Geoscience and Remote Sensing. Vol. GE-25. No. 2. Pp. 159-173. Doi: 0196-2892/97/0300-0159

Livingstone, C.E. 1991. Springtime C-band SAR backscatter signatures of Labrador Sea marginal ice: measurements versus modeling predictions. IEEE Transactions on Geoscience and Remote Sensing. Vol. 29. No. 1. Pp. 29-41

Livingstone, C.E. and M. R. Drinkwater. 1991. Springtime C-band SAR backscatter signatures of Labrador Sea marginal ice: Measurements versus modeling predications," IEEE Trans. Geoscience Remote Sensing. Vol. 29, pp. 29-41.

G. A. Maykut. 1978. Energy exchange over young sea ice in the central Arctic. Journal of Geophysical Research. Vol. 83. Pp. 3646-3658.

Maykut, G. and Perovich, D. 1987. The role of shortwave radiation in the summer decay of a sea ice cover. Journal of Geophysical Research. Vol. 92. No. C7. Doi: 10.1029/0JGREA0000920000C7007032000001. issn: 0148-0227

Morey, R.M.; Kovacs, A. and G.F.N. Cox. 1984. Electromagnetic properties of Sea Ice. Cold Regions Science and Technology. Vol. 9. Issue. 1. Pp. 53-75

Nghiem, S.V.; Rigor, I.G.; Provich, D.K.; Clemente-Colón, P.; Weatherly, J.W. and G. Neumann. 2007. Rapid Reduction of Arctic Perennial Sea Ice. Geophysical Research Letters. Vol. 34. L19594. DOI:10.1029/2007GL031138

Nghiem, S.V. and C. Bertoia. 2001. Study of multi-polarization C-band backscatter signatures for Arctic sea ice mapping with future satellite SAR. Canadian Journal of Remote Sensing, Vol. 27, No. 5, Pp. 387–402.

Nghiem, S.V.; Martin, S.; Perovich, D.K.; Kwok, R.; Drucker, R.; and Gow, A.J. 1997. A laboratory study of the effect of frost flowers on C band radar backscatter from sea ice. *Journal of Geophysical Research 102(C2): doi: 10.1029/96JC03208. issn: 0148-0227.*

Onstott, R. and Shuchman, R. 2004. Chapter 3: SAR Measurements of Sea Ice *from* Synthetic Aperture Radar Marine Users Manual. National Oceanic and Atmospheric Administration (NOAA). Washington, DC.

Petrich, C. and H. Eicken. 2010. Sea Ice. 2nd Edition. Wiley-Blackwell. Chapter 2: Growth, Structure and Properties of Sea Ice.

Rigor, I.G. and J.M. Wallace. 2004. Variations in the age of the Arctic Sea ice and summer sea ice extent. Geophysical Research Letters. Vol. 31. L09401. DOI: 10.1029/2004GL019492

Rothrock, D. A., Y. Yu, and G. A. Maykut. 1999. Thinning of the Arctic sea-ice cover. Geophysical Research Letters. Vol. 26. No. 23. Pp. 3469-3472.

Sandven, S. and O.M. Johannessen. 2006. Sea Ice Monitoring by remote sensing. In: J. Gower (ed.). Remote Sensing of the Marine Environment (Manual of Remote Sensing, 3rd edn. Vol. 6. Pp. 241-283. American Society for Photogrammetry and Remote Sensing, Bethesda, MD.

Scharien, Randall K.; Geldsetzer, T.; Barber, D. G.; Yackel, J.J. and Langlois, A. 2010. Physical, dielectric, and C band microwave scattering properties of first-year sea ice during advanced melt. Journal of Geophysical Research. Vol 115. C12026. Doi: 10.1029/2010JC006257

Soh, L.K. 1999. Texture Analysis of SAR sea ice imagery using gray level co-occurrence matrices. IEEE Transactions on Geoscience and Remote Sensing. Vol. 37. No. 2. Pp. 780-795

Stofan, E.R. 1995. Overview of result of Spaceboune Imaging Radar-C, X-Band Synthetic Aperture Radar (SIR-C/X-SAR). IEEE Transactions on Geoscience and Remote Sensing. Vol. 33. No. 4. Pp. 817-828

Stroeve, J.; Holland, M.M.; Meier, W.; Scambos, T. and M. Serreze. 2007. Arctic Sea Ice Decline: Faster than Forecast. Geophysical Research Letters. Vol. 34. L09501. DOI: 10.1029/2007GL029703

Tucker, W.; Perovich, D.K.; Gow, A. J.; Weeks, W. F. and M. R. Drinkwater. 1992. Microwave Remote Sensing of Sea Ice. American Geophysical Union. Vol. 68. Chapter 2: Physical properties of sea ice relevant to remote sensing.

Turner, J.; Overland, J.; Walsh, J. 2007. An Arctic and Antarctic Perspective on Recent Climate Change. International Journal of Climatology. Vol. 27. No. 3. Pp. 277–293.

Ulaby, F.T.; Moore, R. K. and A. K. Fung. 1986. Microwave Remote Sensing: Active and Passive. Norwood, MA. Artech House Inc. Vol. 3.

Warner, K., Iacozza, J., Barber, D.G. On the Classification of the Melt Season First-Year and Multiyear Sea Ice in the Beaufort Sea Using Radarsat-2 Data. International Journal of Remote Sensing. (in review). *Manuscript ID. TRES-PAP-2012-0529*

CHAPTER FIVE: CONCLUSIONS AND RECOMMENDATIONS

5.1 Summary

The overall purpose of this study was to improve understanding of the relationship between the geophysical state of sea ice and the microwave signatures of advanced melt sea ice from the Radarsat sensor and/or an *in situ* C-Band scatterometer. Firstly, this was addressed by an investigation regarding the geophysical properties of sea ice in the late summer melt season; this included an in depth examination of the geophysical properties of first year and multiyear sea ice in chapter two, as well as brief discussions of *in situ* ice characterization in chapters three and four. This analysis showed us that the geophysical properties of both FYI and MYI are changing; particularly in the summer season, FYI salinity profiles are different than historical profiles due to warmer ocean and atmospheric temperatures. Chapter two provided a background and contextual information on the research topic relevant to active microwave remote sensing of sea ice. This chapter included a discussion on the formation, melt, salinity characteristics and structure of first year and multiyear sea ice, the thermodynamic properties of sea ice, how these geophysical features affected the microwave backscattered signatures, and finally a discussion of the instruments used to obtain microwave backscattered signatures, including the Radarsat-2 sensor and an *in situ* C-Band scatterometer. The second main thesis objective was addressed in chapter three by quantifying the microwave scattering differences between FYI and MYI in the late melt season, and discuss potential solutions to increase their discrimination using new and emerging SAR technologies. The third and

final objective of this thesis included an exploration on how small temperature changes affect the *in situ* multiyear sea ice microwave signatures in the summer season over a diurnal period and if these changes were captured in Radarsat-2 data.

The results from chapter three presented the difficulties of using Radarsat-2 data for summer ice classification by quantifying of the microwave scattering differences between FYI and MYI in the late melt season and exploring the role of polarization and incident angles in their discrimination. A statistical analysis was done to investigate if there were optimal polarizations (HH versus HV) or incident angles for differentiating ice types in the advanced melt season. *In situ* characterization of FYI and MYI showed minimal differences in the physical properties for the two distinctly different ice types, creating similar microwave signatures obtained from Radarsat-2, thus making them difficult to differentiate. When comparing the σ° frequency distributions (dB) from the different polarizations (HH versus HV), as well as the various incidence angles (20°, 35° and 45°), they were all statistically different ($p<0.05$), confirming that polarization and incident angles govern the scattering behaviour and that they may aid in the differentiation of the different sea ice types during the melt season. A comparison of the ice types (FYI versus MYI) was also conducted, and the co-polarized data were proven to be statistically indistinguishable ($p>0.05$), however, the cross-polarized data (HV) was proven to be statistically different ($p < 0.05$), implying ice type also has a significant affect on the σ° signatures obtained from the Radarsat-2 data. The results from this paper can be used for algorithms and for modeling studies to improve machine and human classification of Radarsat-2 data of this late season ice.

The investigation of advanced melt season microwave scattering signatures was continued in chapter four. The results from this chapter included a discussion of the effects of small scale temperature changes (less than three degrees Celsius) on scattering signatures and whether there were optimal incidence angles, polarizations or times of day required to maximize ice floe discrimination. The results from this study found that there was an inverse relationship between temperature and the microwave scattering signatures, meaning as temperatures increased, the signatures decreased. This shows the strong temperature (and phase) dependence of water on active microwave scattering. The investigation into the best combination of incidence angle and polarization consistently showed that co-polarized data (HH or VV) at the lower incidence angles is most effective in detecting melt in the data. An analysis at larger spatial scales using Radarsat-2 data to determine if there was an optimal time of day to discriminate floes from the data led to the discovery that morning overpasses had consistently higher backscattered values than the evening overpasses, meaning data collected from these would be better for ice classification. Investigation of larger spatial scales using Radarsat-2 data showed that there was little spatial variability in the signatures, yet a significant amount of temporal variability. The analysis also showed that diurnal microwave signatures were highly variable during the advanced melt season and that small temperatures changes can cause significant changes in the C-Band scatterometer signatures.

Effective detection and classification of ice types during the summer season has proven to be extremely difficult. This M.Sc. research has provided additional knowledge on the differentiation of MYI from FYI using *in situ* geophysical data, *in situ* C-Band scatterometer data and Radarsat-2 data during the advanced melt season. This is a crucial

season for ice differentiation, as there is increased shipping and hydrocarbon exploration throughout the area. This research also showed that it's not only seasonal variation in signatures that cause this difficulty, but even within a diurnal cycle, there are large changes in signatures. The insights from this thesis will contribute towards more accurate estimations and classifications of sea ice in the advanced melt season using microwave data; these are extremely important considerations when attempting to understand how the Arctic marine icescape will respond to future changes as a result of climate change.

5.2 Future Recommendations

This thesis has examined the scattering signatures of sea ice obtained from active microwave sensors, including the propagation and the scattering that occurs within sea ice.

While doing the field work necessary for this study, many challenges and difficulties were encountered with *in situ* physical data collection associated with scatterometer data and the availability of coincident satellite imagery. Due to the remoteness of the sites used to conduct this research, a ship-based platform was needed in order to conduct our work; the CCGS *Amundsen* provided numerous opportunities to perform both on ice operations as well as scan the ice surface using the C-Band scatterometer. There were however limitations with ship based work, including: the dependence of the site on the ship location, timing limitations, and difficulties in keeping the ship motionless, which was necessary when scanning the surface of the ice using the C-Band scatterometer. Although critical measurements were collected, the classification of sea ice was hindered by some of the logistics related to ship based field work. Future experiments can improve on the knowledge of scattering during the summer season, as

well as changes in the physical processes of sea ice during the summer season that cause a change in the scattering.

Further experimentation on microwave remote sensing of sea ice includes the need to gain a better understanding of the ice conditions during the advanced melt season. Some recommendations for further research include:

- Continued on-ice work is required to gain a better understanding of the processes which govern the distribution of water in liquid phase within the MY and FY surface/volume. It is this distribution of liquid water which dominates the microwave signatures and advanced knowledge of how and why water moves within MY and FYI ice types will benefit their segmentation.
- Conduct an in depth diurnal study which involves a collection of numerous parameters, including air temperature, surface temperature, dielectric properties of ice, salinity profiles of ice, and incoming and outgoing solar radiation. It would be beneficial to have an ice camp to set up the necessary equipment and have a study dedicated to the effect of atmospheric changes on microwave scattering signatures.
- Investigate systems with other frequencies to gain a better understanding of how the interaction of microwaves at the surface of sea ice occurs. This should include an in depth study focusing on the L-Band frequency or X-band.
- Take the increased knowledge of advanced melt ice conditions and use it to develop algorithms that would take into consideration the correlations between temperature and backscattered signatures and help create automated detection of ice types during the summer season.

These recommendations would significantly add to the knowledge base of active microwave remote sensing of sea ice. Improved understanding of the physical properties and the processes that are occurring in the late melt season would help image analysts with the classification of ice types using spaceborne synthetic aperture radar (SAR) data, and as a result, this would make shipping and hydrocarbon exploration through the Arctic summer season safer.